Project Acronym:

SOUNDPET(INTEGRATED/0918/0008)

MRI-guided Focused ultraSOUND system for cancer in PETs (dogs and cats)

Deliverable number: 6.2

Title: Evaluation of the accuracy of the robotic system

Prepared by:

Theocharis Drakos (MEDSONIC)
Marinos Giannakou (MEDSONIC)
Christakis Damianou (CUT)
Anastasia Antoniou (CUT)
Nikolas Evripidou (CUT)
Christakis Damianou (CUT)
Theodora Christodoulou (GOC)
Natalie Panayiotou (GOC)
Leonidas Georgiou (GOC)

Date: 12/02/2021

Ευρωπαϊκή Ένωση
Ευρωπαϊκά Διαρθρωτικά και Επενδυτικά Ταμεία

Κυπριακή Δημοκρατία

Διαρθρωτικά Ταμεία
της Ευρωπαϊκής Ένωσης στην Κύπρο

Table of Contents

Executive summary

In this deliverable (6.2), the accuracy of the motion of the 4 DOF robotic systems is described. The accuracy of linear motion in all axes (X-, Y-, and Z-axis), as well as the accuracy of angular motion (θ-axis), were initially tested using digital calipers and specially designed 3D-printed parts for both robotic systems (version 1 and 2). The special parts were designed to attach the digital calipers to the several motion stages for performing accurate measurements. The experimental set-up utilized to measure the motion accuracy of the robotic device in each axis is explained in detail. The electronic systems that were developed for controlling robotic motion using an Arduino microcontroller and a digital acquisition card accompanied with the relevant software of the robotic devices are also described. The accuracy of the linear axes was estimated at step movements of 1 mm, 5 mm, and 10 mm. The accuracy of the angular motion was assessed at step angles of 1^o, 5^o and 10^o. The motion error of each axis of each robotic device was estimated. In addition, the speed of motion of the robotic system version 1 was calculated. MRI was also used to assess the accuracy of motion of the robotic system version 2 in two linear axes (X and Y). For these experiments, the robotic device was sited on the MRI couch and a plastic marker was mounted on the top of the FUS transducer so that it was visualized in MR images. Lastly, a third method was used for evaluating the motion accuracy visually. The method involved performing multiple ablations in transparent plastic films by moving the transducer of the robotic system version 2.

Introduction

The introduction of robots in medicine has been essential for establishing minimally invasive diagnostic and therapeutic modalities by extending their benefits to most surgical specialties [1]. Robotic devices are continuously being invented to aid in the positioning and manipulation of surgical instruments and energy sources. Such robotic-assisted procedures require a highly accurate operation to approach a target in a minimally invasive manner and meet the clinical requirement. Simultaneously, the accuracy data is essential for establishing safety guidelines for clinical applications.

All the techniques used to test the mechanical accuracy of a robot are based on the idea of comparing the commanded motion step with the actual displacement as estimated by a distance-measuring technique. Mechanical accuracy refers to both the positioning and repeatability accuracy of motion. Before the procedure is applied and evaluated *in vivo*, accuracy assessment is typically carried out in free space, sometimes referred to as intrinsic system accuracy, meaning not under real conditions. Most commonly, after acquiring evidence of sufficient accuracy and repeatability by benchtop testing, the system is evaluated in the environment that is intended to be clinically used, such as the bore of an MRI system. This is essential for ensuring that the system maintains a high degree of accuracy in real-like scenarios. Even a minimal magnetic shift of the system's components in the MRI could affect the accuracy and compromise the patient's safety in highly sensitive procedures.

In the framework of assessing the accuracy of motion in a free robot workspace, in a benchtop setting, several motion tracking techniques were proposed [2–7]. Optical tracking systems have been widely used for confirming adequate targeting accuracy for needle-related interventions, where the placement error is defined by the deviation of the actual tooltip position from the desired location [2–5]. The accuracy of an automated robot intended for breast biopsy in precisely reaching a target was evaluated using a rigid test tool, which was driven to target positions through straight and angled paths and monitored with an optical tracker [2]. Similarly, Patriciu et al. [3] investigated the motion accuracy of a system for automated brachytherapy seed placement using an optical tracking system. An active marker was mounted on the end-effector of the robotic arm allowing continuous tracking of its position. An optical tracking system was also used by Patel et al. [4], who evaluated a robotic system intended to perform shoulder arthrography. A specially designed frame with optical markers served as the reference, while a tracking structure was also integrated on the needle guide so that its position

can be tracked relative to the reference frame [4]. A different tracking method was chosen by Dou et al. [5], who measured the positioning accuracy of a brachytherapy system using a 3D laser tracker, as well as an inertial measurement unit [5]. An optical measuring microscope has also been proposed for estimating the actual displacement of a linear motion stage after the execution of commanded movements of varying motion steps in both forward and reverse directions [6]. In another study [7], the displacement of an endoscope manipulator was measured with two Charge-Coupled Device (CCD) laser micrometers.

More straightforward methods involving the use of digital calipers and special structures have also been carried out in the laboratory environment for accuracy evaluation purposes. The needle tip accuracy of a breast biopsy robot was evaluated in free air by targeting crosshairs drawn on a board [8]. The needle tip was commanded to puncture these targets, which were vertically positioned, and the error was estimated by the distance from the center of each target to the corresponding pierced hole [8]. Similarly, in the framework of evaluating the motion accuracy of a robot intended for transcranial focused ultrasound (FUS) surgery, the FUS transducer was replaced by a felt-tipped pen, which was commanded to touch multiple resolution points distributed on three perpendicular planes demonstrating the entire robot's workplace [9]. Each created mark was assigned in resolution circles, which included radial and angular approximation zones for facilitating targeting error measurement. Another simplified method involves mounting digital calipers on the motion stages of a robot such that their actual displacement after motion execution can be directly measured by the incremental distance of the caliper [10-11].

After assessing the accuracy of needle-related interventions in free space, experiments under more realistic conditions are typically performed. Initial experiments are predominantly performed in phantoms in an imaging environment, involving the use of fiducial markers for visualizing and registering the system in the imaging coordinates. A first planning scan is acquired for selecting the target locations in the phantom and calculating the insertion parameters [12–14]. Following targeting according to the estimated coordinates exported to a motor controller software, confirmation images are collected for assessing the accuracy of needle placement relative to the prescribed locations [12–14]. Patel et al. [12] reported a phantom study performed under real-time MRI guidance, where a needle-based therapeutic ultrasound applicator was robotically inserted in a gelatin phantom in locations predefined in 3D Slicer. The intended probe tip position was compared to the actual position as visualized in 3D-Fast Field Echo (FFE) images. Likewise, Krieger et al. [13] assessed the accuracy of motion

of a system for prostate interventions in a prostate phantom. The rectal sheath was automatically aligned with the desired insertion point and then manually inserted in the phantom. The void caused by the needle tip was visualized in axial Turbo Spin Echo (TSE) proton density images enabling calculation of the in-plane error of targeting. Targeting accuracy assessment in MRI was also performed in air with the use of a gadolinium filled virtual needle, which was tracked and visualized using T1-weighted Isotropic Volume Examination sequence [14].

Robotic devices intended for non-invasive FUS applications are constantly being developed [15] and extensively evaluated by performing ablation studies, in which the separation precision of multiple ablations constitutes an indication of the positioning error. Tao Wu et al. [16] performed quality control of a FUS system, where the focus positioning accuracy was tested by performing multiple sonications on a Lucite cart. The transducer was accommodated in a water tank to be acoustically coupled to the target. Left-right and superior-inferior movements by specific distance were commanded by a treatment planning software, resulting in numerous sets of melted spots arranged in discrete patterns. The actual distance between adjacent spots was measured with a digital caliper. In other phantom experiments conducted in a benchtop setting [10], the linear motion stages were commanded to create discrete ablations of specific spacing in a gel phantom. White coagulation lesions were clearly visible being spaced by the desired step, thus confirming the accuracy of positioning.

Price et al. [9] followed a similar approach but in an MRI setting. An MR conditional robot for transcranial FUS interventions was used to perform multiple sonications in a 2 x 3 pattern in a heat-sensitive gel phantom located in a water tank. The thermal images acquired after each sonication were superimposed onto one image, and the positioning accuracy was defined as the spacing between the centers of adjacent ablated areas [9]. This technique was also selected for evaluating the accuracy of motion of an MR-compatible FUS device intended for brain diseases treatment [17]. A four-point ablation pattern was performed *in vitro*, in lamb brain, with different motion steps of 1 to 10 mm, and the formed lesions were visualized in T1-weighted Fast Spin Echo (FSE) images. The ablated areas appeared as spots of increased signal intensity, and the distance between neighboring ablations was calculated from the center of each spot. Smaller errors were estimated with increasing step distance [17]. Similarly, Yiallouras et al. [11] performed phantom experiments where T2-weighted FSE images revealed areas of reduced signal formed in a discrete pattern. It is notable that Sagias et al. [18] developed a motion phantom for evaluating high intensity focused ultrasound (HIFU) protocols on moving

targets in the MRI environment. In another study carried out in a gel phantom [19], the robotic arm of an US-guided FUS ablation system was commanded to move the focal point to ablate the four corners of the phantom, and the targeting accuracy was evaluated by visualizing the sonicated areas on US images.

In this deliverable, we present three simple methods that were used for assessing the accuracy of motion of the Magnetic Resonance guided FUS (MRgFUS) robotic systems in both benchtop and MRI environments. The system is intended for ex-vivo and in-vivo preclinical use, including studies in companion animals of all sizes with naturally occurring tumours. The motion accuracy of the robotic system version 1 was only evaluated using digital calipers. In the first method, a digital caliper was mounted on the motion stage under evaluation with the assistance of specially designed 3D printed parts, having its one edge fixed on a stationary part and the other on a movable part. In that way, a specific step movement of the stage results in an analogous increment in the caliper. The motion accuracy of the robotic system version 2 was also evaluated using MRI and visual methods. Specifically, the second evaluation procedure relates to accuracy assessment in the MRI setting. The robotic device was sited on the MRI couch, and a plastic marker was mounted on the top of the FUS transducer so that it can be visualized in MR images. The third method involves performing multiple ablations in a transparent plastic film by robotic movement of the transducer.

Evaluation using digital calipers

Evaluation of the robotic system version 1

Four DOF robotic system version 1

The motion accuracy of the robotic system version 1 was evaluated using digital calipers. The robotic system includes four axes, three axes for linear motion (X, Y, and Z) and one for angular motion (Θ). The computer-aided design (CAD) drawing of the fully assembled 4 DOF robotic device with the motors (USR30-S3N, Shinsei Corporation, Kasuya Setagaya-ku, Tokyo, Japan) is shown in Figure 1. The direction of each axis of the positioning mechanism is indicated (Figure 1a). All the components, which have been assembled to develop the robotic system, are described in detail in Deliverable 3.1 (Four DOF robotic system-version 1).

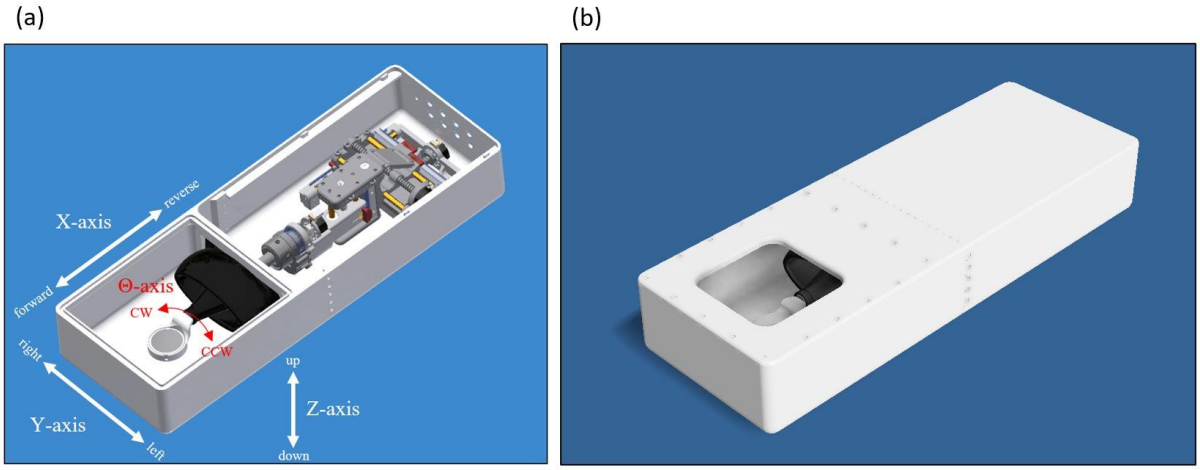

Figure 1: CAD drawing of the 4 DOF robotic system version 1 a) without the cover, and b) with the cover.

Each motion stage of the robotic device is PC-controlled through a special software. Due to the constraints of the MRI bore, there are some spatial limits. The maximum distance that the transducer holder can move, from the one end to the other, is 55 mm in the X-axis, 76 mm in the Y-axis, and 28 mm in the Z-axis. The rotation limit is 180 degrees, 90 degrees clockwise (CW) and 90 degrees counterclockwise (CCW).

Electronic system

The electronic driving system was composed of an Arduino microcontroller, motor encoders, and a power supply. The electronic system is described in detail in Deliverable 3.3 (Electronic driving system) and it is shown in Figure 2.

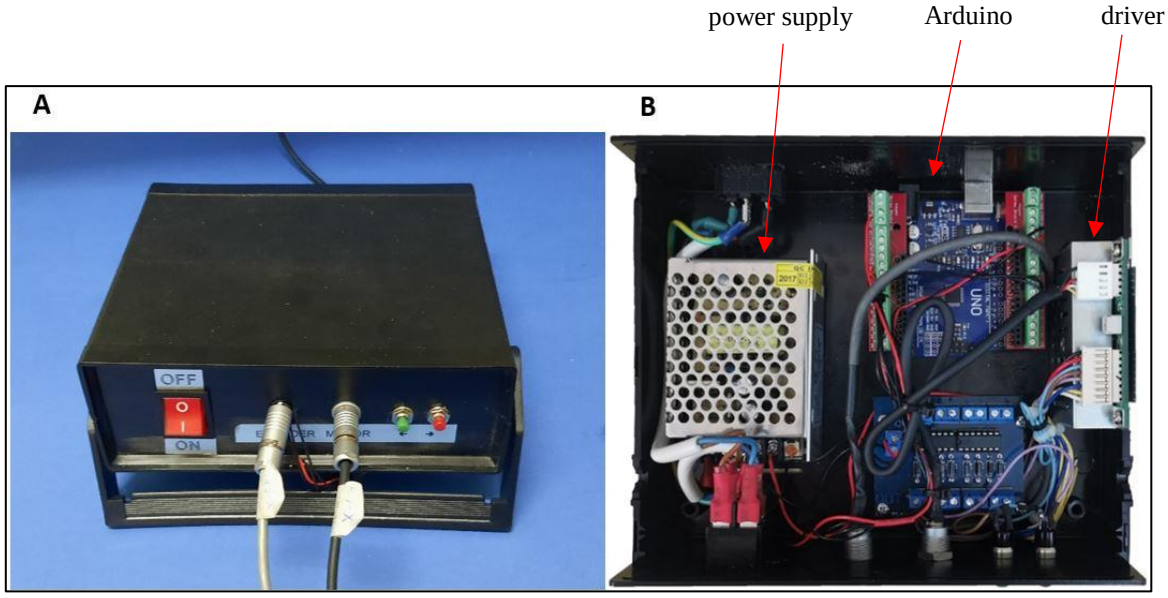

Figure 2: a) The electronic driving system of the robotic device, and b) the inner part of the electronic system indicating the main components. This system controls a single motion stage. A different electronic system that controls all the axes of the robotic system was also developed.

Software

The piezoelectric motors and the encoders of the robotic device are connected through the electronics to a specially designed software. A screenshot of the software is shown in Figure 3. The connection of the software with the motors and encoders was achieved through an Arduino microcontroller (Uno SMD R3). Specifically, the software was able to send commands to the microcontroller and communicate with the motors and encoders of the robotic system. The software has many capabilities including functionality for commanding and monitoring motion of the robotic device. Basically, measurement of the motion accuracy of the robotic system gives an indication of the motion accuracy of the piezoelectric motors and the correct motion reading by the encoders.

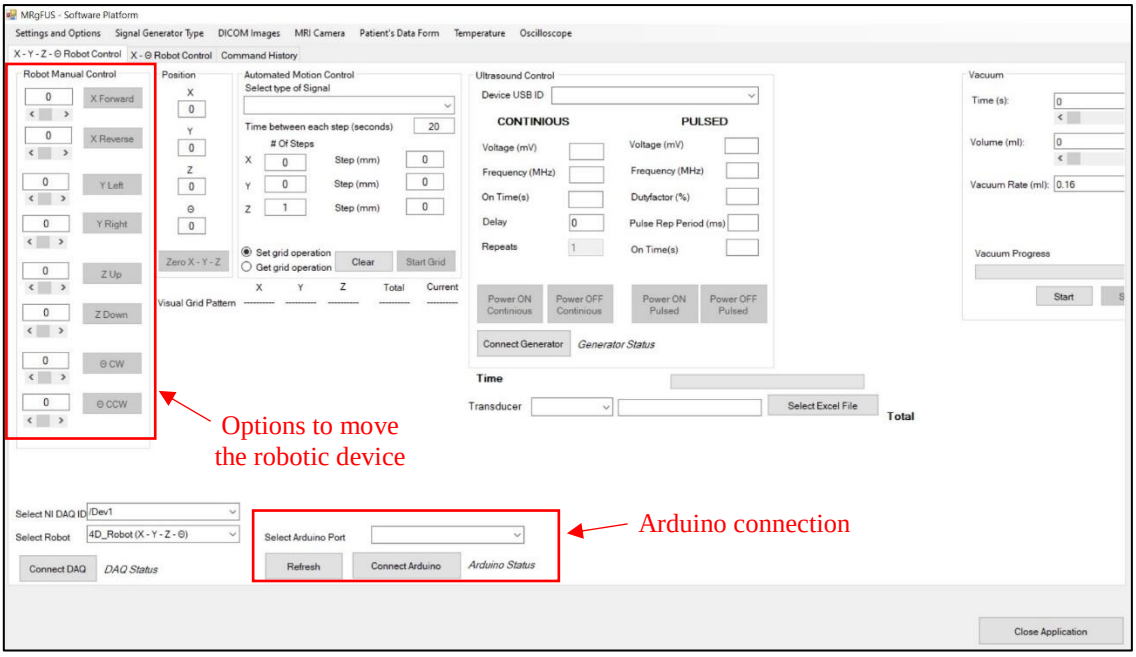

Figure 3: Main interface of the software. The robotic device's movement options are highlighted.

Evaluation of the X-axis

The accuracy of the motion in the X-axis was evaluated using a digital caliper (ROHS NORM 2002/95/EC) and additional 3D-printed parts. The special parts were designed to be easily attached to the robotic device, provide stability to the digital caliper, and allow for accurate measurement. The several parts were printed on a 3D printer (F270, Stratasys, 7665 Commerce Way, Eden Prairie, Minnesota, 55344, USA) using ABS (Acrylonitrile Butadiene Styrene) material. Figure 4 shows the digital caliper that was used in these experiments, and Figure 5 shows the CAD drawing of the parts that were designed for evaluating the motion accuracy in the X-axis. These parts were easily attached to the robotic device.

Figure 4: Digital caliper that was used to evaluate the X and Y linear motions of the robotic system.

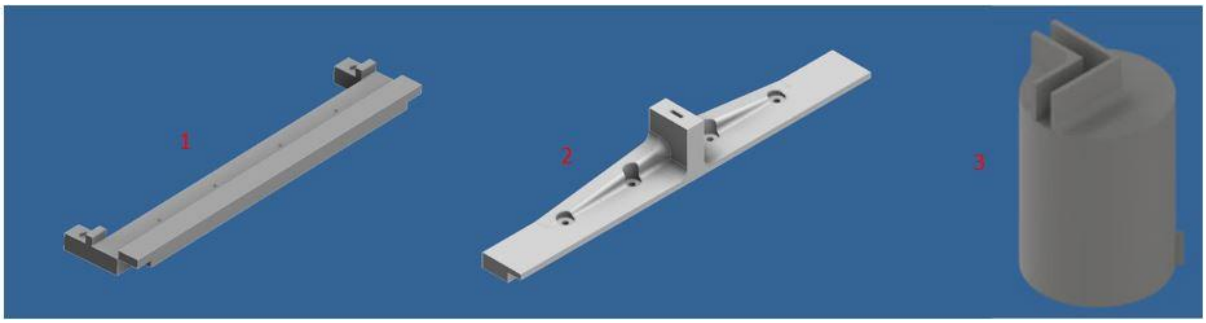

Figure 5: CAD drawings of the parts that were used to evaluate the X-axis motion.

Figure 6 shows the CAD drawing of the set-up that was used to estimate the accuracy of the X-axis motion attached to the robotic device. The corresponding photo of the experimental set-up is shown in Figure 7.

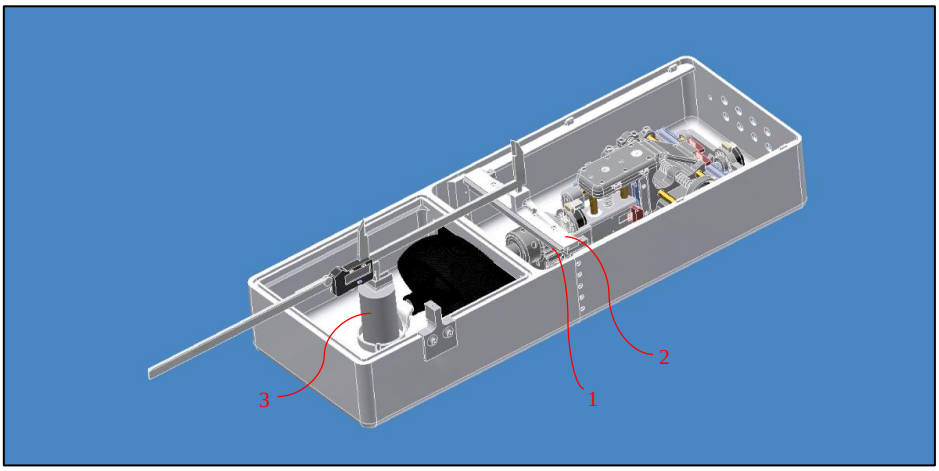

Figure 6: CAD drawing of the setup that was used to estimate the accuracy of the X-axis motion.

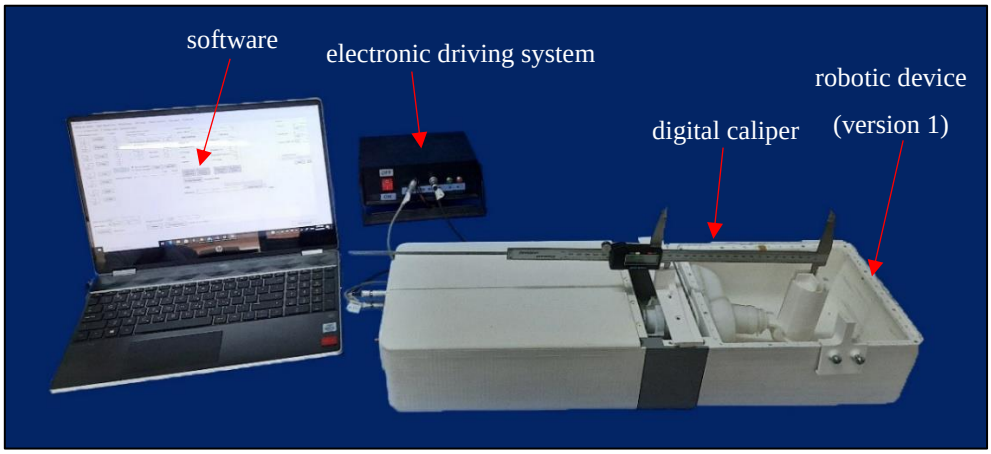

Figure 7: Photo of the experimental set-up used to evaluate the accuracy of the X-axis motion of the robotic device version 1.

The accuracy of the motion in the X-axis was evaluated in the forward and reverse directions, as shown in Figure 8. The robot was moved by a certain distance using the motion commands of the software and the actual distance of motion (displacement) was recorded by the digital caliper. Motion steps of 1, 5, and 10 mm were evaluated. Notably, the robotic device comprises a plastic bellow that is used to permanently seal the container where the transducer is actuated, and which is filled with water during transducer activation, so as to protect the mechanical components of the system. The bellow has a special design that enables free movement of the transducer in all incorporated axes. Table 1 lists the actual measured distance at commanded motion steps of 1, 5, and 10 mm in the X-axis. Figure 9 to Figure 11 show bar charts of the measured distance for bidirectional steps of 1, 5, and 10 mm in the X-axis, respectively, with respect to the repetition number for 20 repetitions. Accordingly, Figure 12 shows the mean values of the actual measured distance versus the intended distance for the X-axis forward and reverse motion.

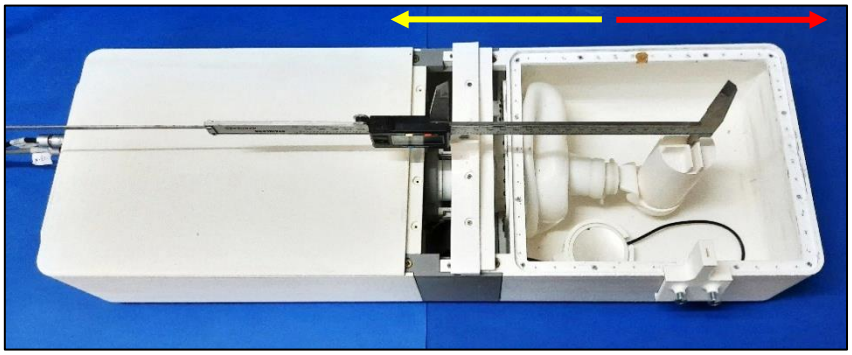

Figure 8: Evaluation of the motion accuracy of the robotic device in the X-axis. The red arrow indicates the forward direction and the yellow arrow indicates the reverse direction.

Table 1: List of distance measurements taken at motion steps of 1, 5, and 10 mm for the X-axis evaluation.

Intended distance (mm)	1		5		10	
Measurement number	**Distance moved forward (mm)**	**Distance moved reverse (mm)**	**Distance moved forward (mm)**	**Distance moved reverse (mm)**	**Distance moved forward (mm)**	**Distance moved reverse (mm)**
1	0.94	0.98	5.00	5.02	10.20	10.03
2	1.06	0.95	5.00	5.05	10.18	10.02
3	1.13	1.13	5.00	5.23	9.88	10.17
4	0.99	1.11	5.02	5.20	10.25	10.22
5	1.04	0.94	5.19	5.14	10.20	10.09
6	1.00	0.98	5.16	5.03	9.90	10.04
7	1.06	1.00	4.96	5.16	10.47	10.44
8	0.97	0.95	5.10	5.19	10.18	10.14
9	0.98	0.9	5.05	5.13	10.20	10.11
10	0.98	0.92	4.90	5.00	10.41	10.19
11	0.99	1.03	5.20	4.97	10.12	10.08
12	1.01	1.12	5.08	5.07	9.98	10.17
13	0.95	0.94	5.09	5.28	10.37	10.28
14	1.00	1.00	5.35	5.18	10.21	10.11
15	1.06	1.03	5.21	5.12	10.10	10.21
16	0.93	0.95	4.87	4.93	10.42	10.39
17	1.03	1.05	5.06	4.93	9.98	10.18
18	1.01	0.93	4.99	5.24	10.07	10.21
19	0.94	1.01	5.10	5.06	10.28	10.33
20	0.94	0.98	5.00	5.02	10.20	10.03
Average	**0.999**	**0.9935**	**5.079**	**5.1055**	**10.1785**	**10.1715**
Standard deviation	**0.0524**	**0.0657**	**0.1174**	**0.1017**	**0.1610**	**0.1160**

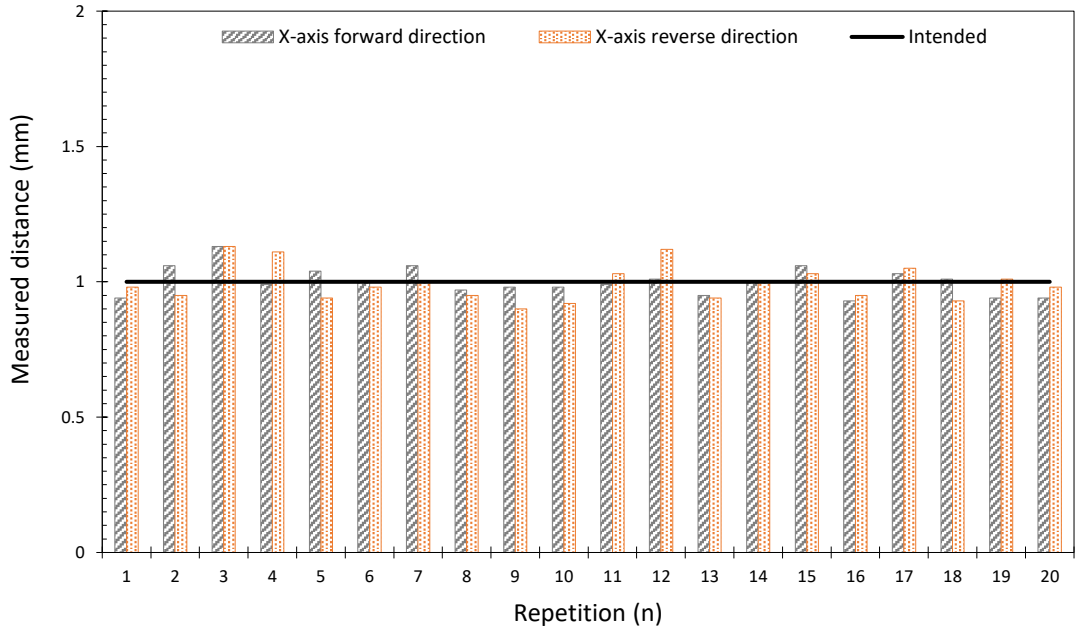

Figure 9: Distance measurements for 20 repetitions for step motion of 1 mm in the X-axis forward and reverse directions. The black straight line indicates the intended distance.

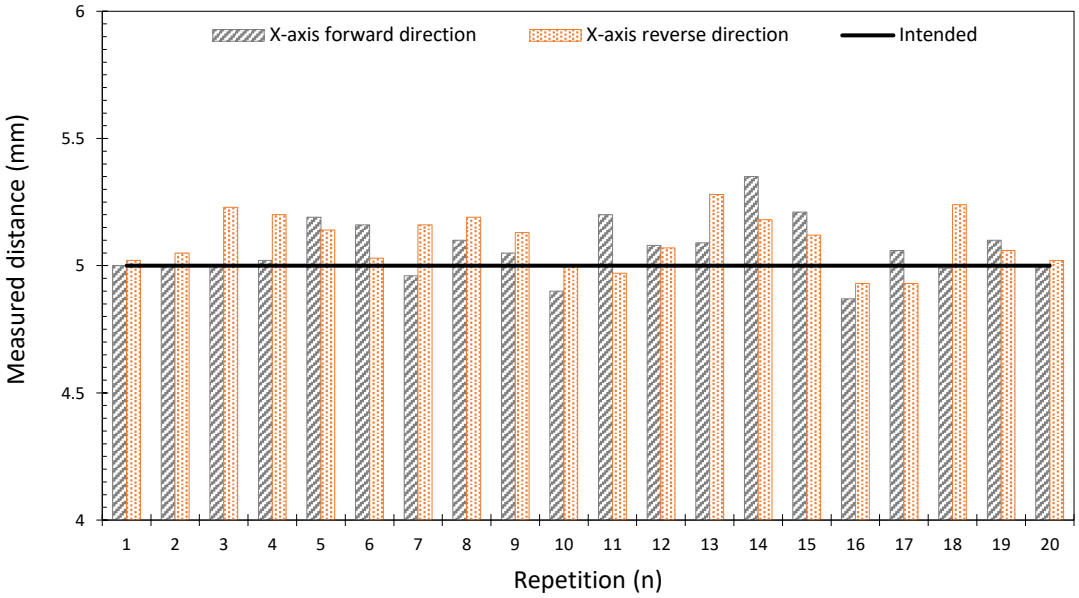

Figure 10: Distance measurements for 20 repetitions for step motion of 5 mm in the X-axis forward and reverse directions. The black straight line indicates the intended distance.

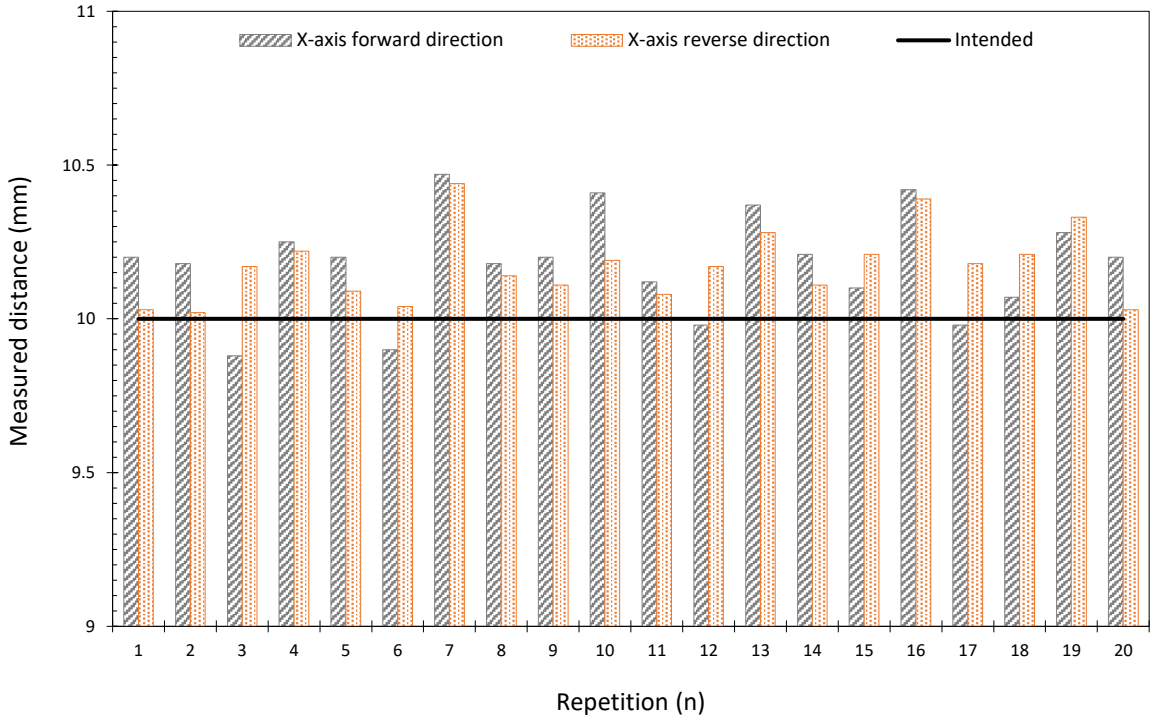

Figure 11: Distance measurements for 20 repetitions for step motion of 10 mm in the X-axis forward and reverse directions. The black straight line indicates the intended distance.

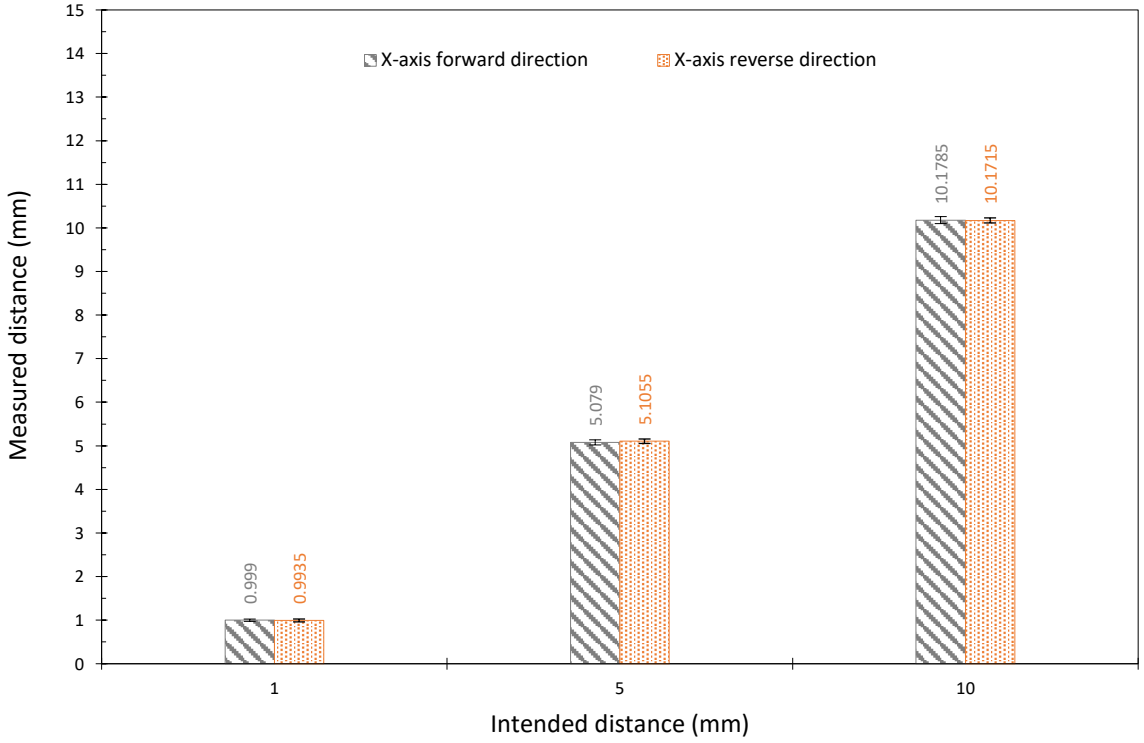

Figure 12: Mean values of the measured distance versus intended distance for the X-axis forward and reverse motion.

The motion error was estimated for each step movement in both X-axis directions. Table 2 summarizes the error values (in μm and percentage) measured at motion steps of 1, 5, and 10 mm for the X-axis forward and reverse directions.

Table 2: List of error estimated at different motion steps for the X-axis forward and reverse directions.

Step (mm)	Error-forward motion (μm)	Error-forward motion (%)	Error-reverse motion (μm)	Error-reverse motion (%)
1	42	4.2	51	5.1
5	47	0.94	65	1.3
10	81	0.81	58	0.58

The speed of the motion of the robotic device in the X-axis was also estimated. Motion steps of different distances (1, 5, 10, and 15 mm) were commanded, and the time needed to cover the commanded distance was calculated. Four measurements were obtained for each motion step and the average speed was calculated (based on the estimated average time). The microcontroller was able to measure the time for which the motors were activated during each motion step. Table 3 lists the time needed for the transducer to cover the various distances, as measured by the microcontroller, and the corresponding speed of motion for the X-axis (forward and reverse directions). The average speed of motion in the X-axis forward and reverse directions is also listed in this table.

Table 3: List of time needed for the transducer to cover different distances and corresponding speed of motion for the X-axis.

Forward direction				
Distance (mm)	**1**	**5**	**10**	**15**
Measurement number	**Time (s) for forward motion**			
1	0.099	0.506	1.032	1.49
2	0.099	0.512	1.018	1.649
3	0.1	0.501	1.046	1.526
4	0.103	0.499	1.027	1.694
Average Time (s)	0.1003	0.5045	1.03075	1.58975
Speed (mm/s)	10.31	10.43	10.01	9.73
Speed of forward direction (average all)	10.12 mm/s			
Reverse direction				
Distance (mm)	**1**	**5**	**10**	**15**

Measurement number	Time (s) for reverse motion			
1	0.104	0.477	0.996	1.547
2	0.102	0.519	1.087	1.685
3	0.094	0.52	1.01	1.58
4	0.104	0.552	1.108	1.732
Average Time (s)	0.101	0.517	1.05	1.636
Speed (mm/s)	10.06	9.80	9.98	9.42
Speed of reverse motion (average all)	9.88 mm/s			

Evaluation of the Y-axis

Figure 13 shows the CAD drawing of the parts that were designed to accurately evaluate the Y-axis motion of the robotic system using a digital caliper.

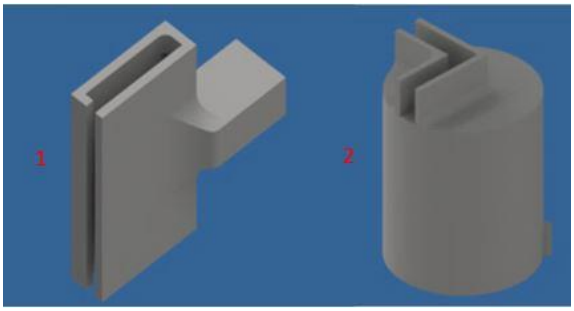

Figure 13: CAD drawings of the parts that were used to evaluate the Y-axis motion.

Figure 14 shows the CAD drawing of the set-up that was used to estimate the accuracy of the Y-axis motion attached to the robotic device.

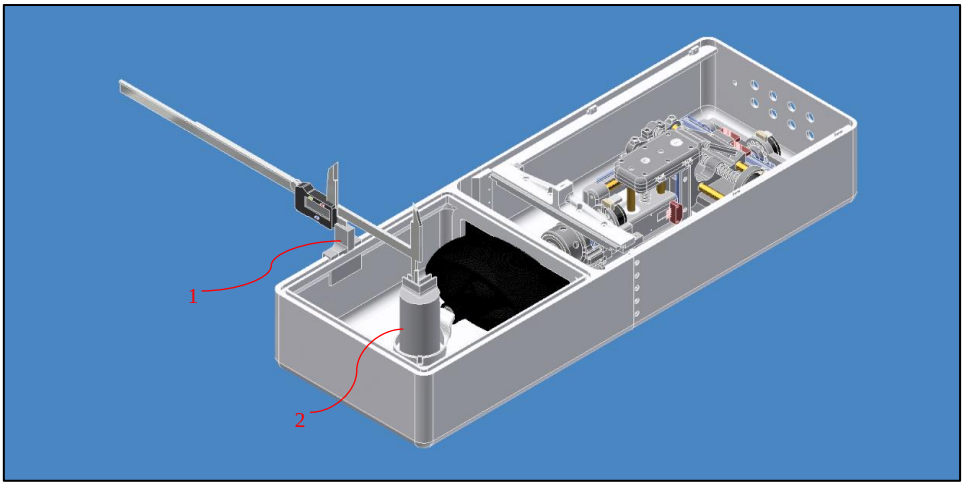

Figure 14: CAD drawing of the set-up that was used to estimate the accuracy of the Y-axis motion.

The accuracy of motion in the Y-axis was evaluated in both left and right directions, as shown in Figure 15. The corresponding photo of the experimental set-up is shown in Figure 16. The robot was moved by certain distances in the Y-axis using the motion commands of the software, and the actual distance of motion was recorded using the digital caliper. Motion steps of 1, 5, and 10 mm were evaluated. Table 4 lists the actual measured distance at commanded motion steps of 1, 5, and 10 mm in the Y-axis. Figures 17 to 19 show bar charts of the measured distance for bidirectional steps of 1, 5, and 10 mm in the Y-axis, respectively, with respect to the repetition number for 20 repetitions. Accordingly, Figure 20 shows the mean values of the actual measured distance versus the intended distance for the Y-axis right and left motion.

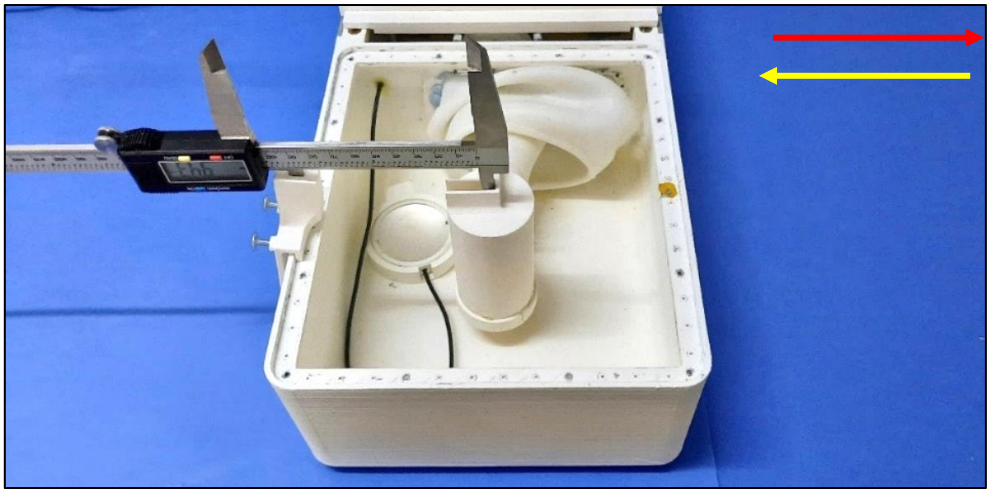

Figure 15: Evaluation of the motion accuracy of the robotic device in the Y-axis. The red arrow indicates the left direction and the yellow arrow indicates the right direction.

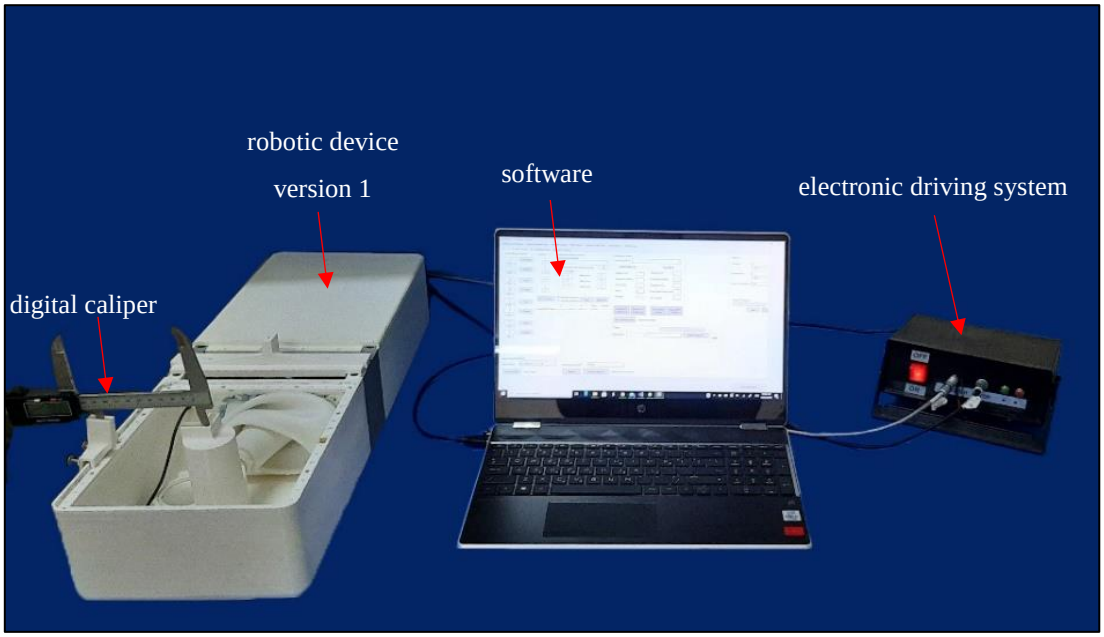

Figure 16: Photo of the experimental set-up used to evaluate the accuracy of the Y-axis motion of the robotic device.

Table 4: List of distance measurements taken at commanded motion steps of 1, 5, and 10 mm for the Y-axis evaluation.

Intended distance (mm)	**1**		**5**		**10**	
Measurement number	**Distance moved left (mm)**	**Distance moved right (mm)**	**Distance moved left (mm)**	**Distance moved right (mm)**	**Distance moved left (mm)**	**Distance moved right (mm)**
1	0.97	1.19	6.61	6.89	9.67	11.11
2	0.96	0.99	5.59	5.00	11.02	9.02
3	0.99	0.74	4.48	4.60	9.45	9.27
4	1.03	0.79	3.83	3.90	9.34	8.4
5	1.02	0.97	5.75	3.79	12.25	12.24
6	0.89	0.83	6.51	4.75	9.04	9.20
7	0.98	1.01	4.49	4.73	9.68	9.42
8	0.93	0.77	4.80	4.69	9.19	8.30
9	0.83	0.83	4.55	4.66	12.38	11.71
10	1.18	0.76	4.86	4.88	9.07	9.08
11	0.92	0.81	4.55	4.25	9.32	8.94
12	0.95	1.05	4.75	5.57	9.19	8.42
13	0.95	0.82	4.36	6.38	11.44	10.35
14	1.09	1.17	7.35	4.19	9.15	9.09
15	0.92	0.86	5.16	4.60	9.09	9.37
16	0.98	1.04	4.28	4.56	9.25	8.02
17	0.78	0.98	4.66	4.52	9.58	10.73
18	0.96	0.92	4.77	4.64	9.24	8.86
19	0.84	0.90	4.75	4.83	9.29	9.17
20	1.06	1.06	4.64	3.45	9.02	8.05
Average	**0.9615**	**0.9245**	**5.037**	**4.744**	**9.783**	**9.4375**
Standard deviation	**0.089**	**0.1313**	**0.8666**	**0.7762**	**1.0426**	**1.1581**

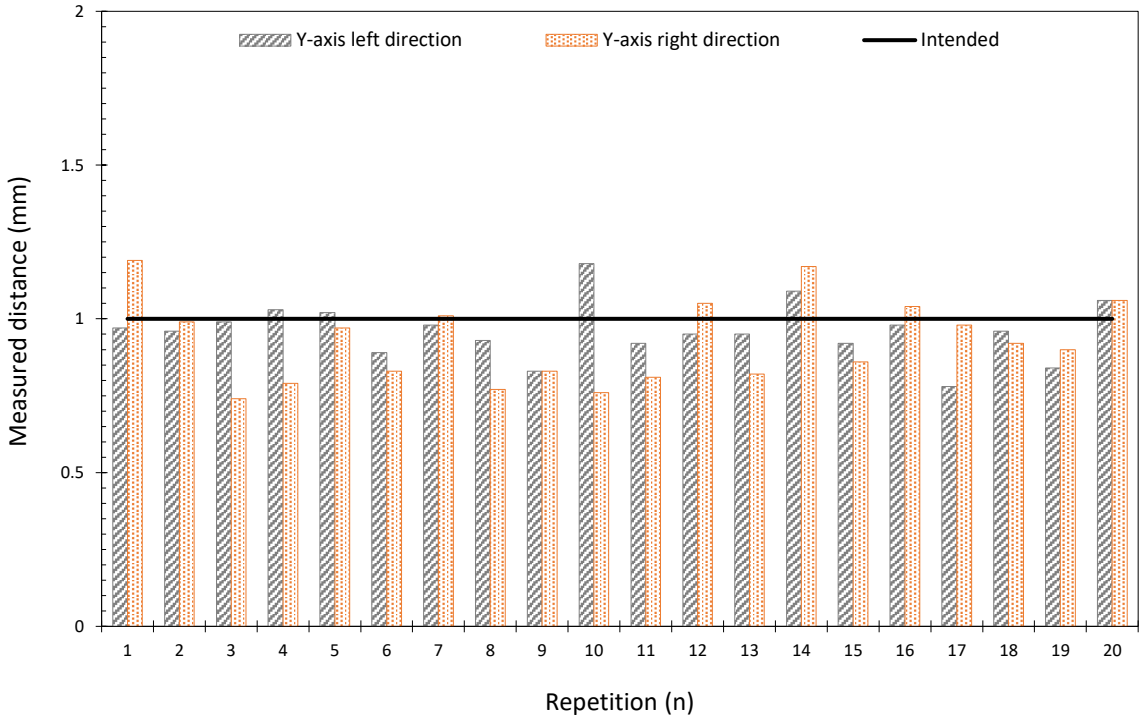

Figure 17: Distance measurements for 20 repetitions for step motion of 1 mm in the Y-axis left and right directions. The black straight line indicates the intended distance.

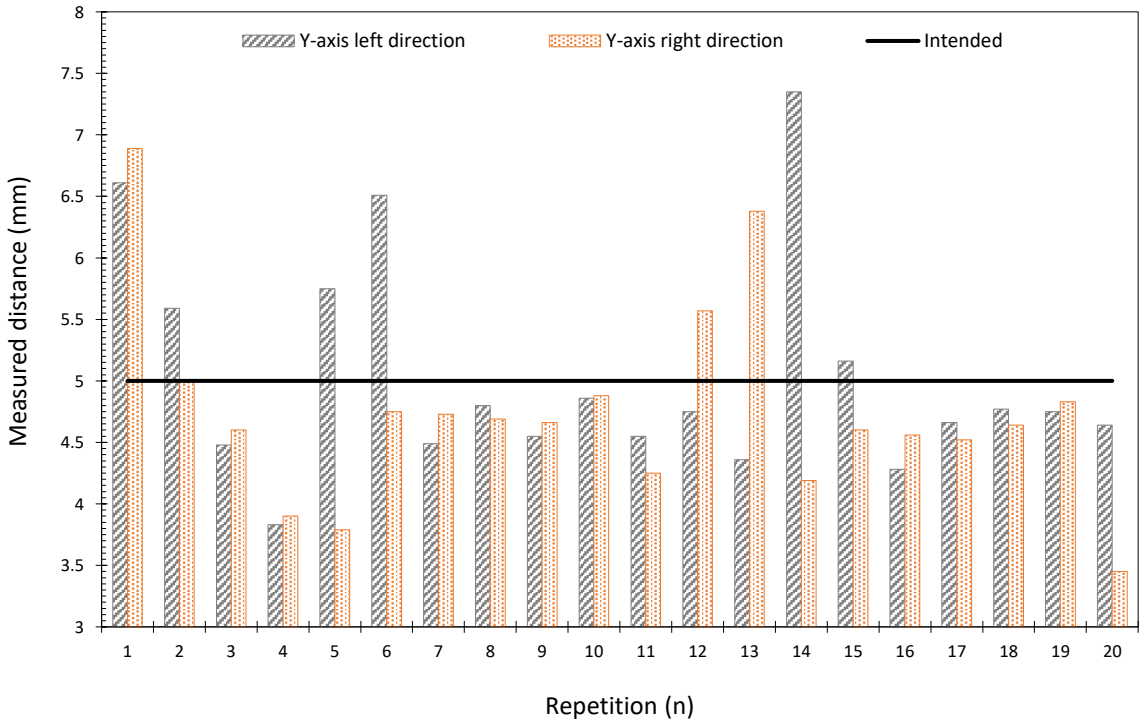

Figure 18: Distance measurements for 20 repetitions for step motion of 5 mm in the Y-axis left and right directions. The black straight line indicates the intended distance.

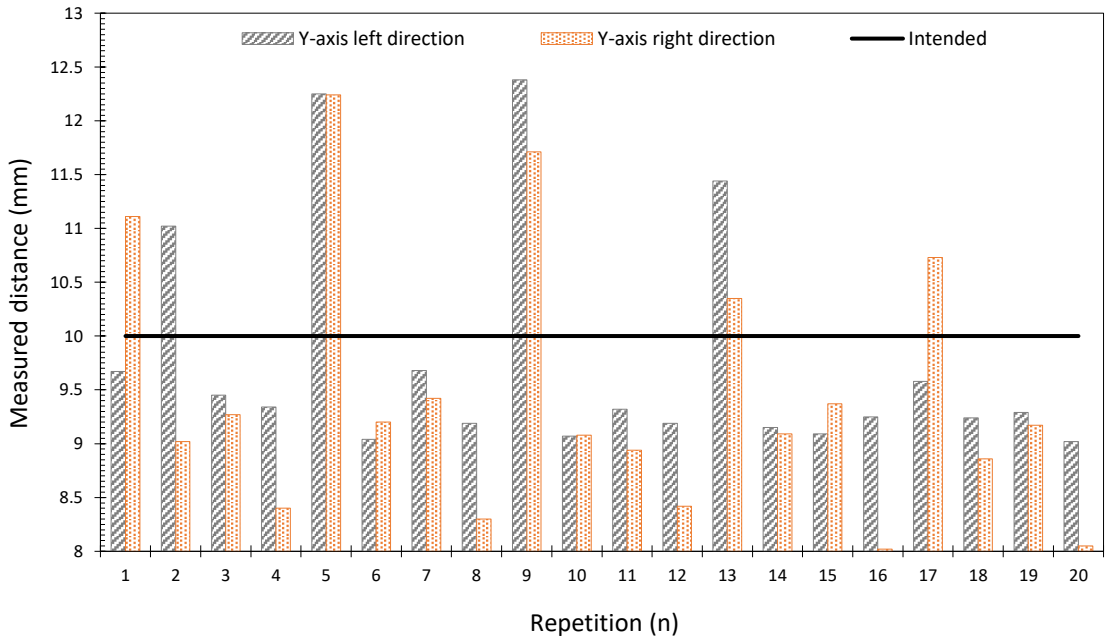

Figure 19: Distance measurements for 20 repetitions for step motion of 10 mm in the Y-axis left and right directions. The black straight line indicates the intended distance.

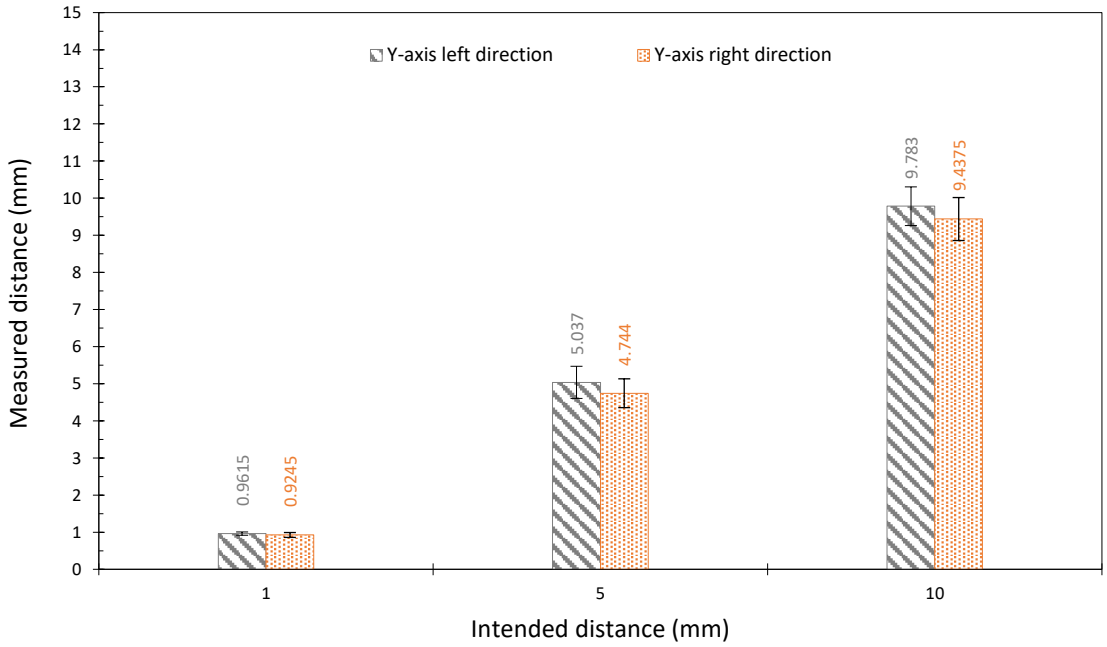

Figure 20: Mean values of the measured distance versus intended distance for the Y-axis left and right motion.

The motion error was estimated for each step movement in both Y-axis directions. Table 5 summarizes the error values (in μm and percentage) measured at motion steps of 1, 5, and 10 mm for the Y-axis left and right directions.

Table 5: List of error estimated at different motion steps for the Y-axis left and right directions.

Step (mm)	Error-left motion (µm)	Error-left motion (%)	Error-right motion (µm)	Error-right motion (%)
1	45	4.5	42	4.2
5	53	1.06	84	1.68
10	123	1.23	86	0.86

The speed of the motion of the robotic device in the Y-axis was also estimated. Motion steps of different distances (1, 5, 10, and 15 mm) were commanded and the time needed to cover the commanded distance was calculated. Four measurements were obtained for each motion step and the average speed was calculated (based on the estimated average time). Table 6 lists the time needed for the transducer to cover the various distances, as measured by the microcontroller, and the corresponding speed of motion for the Y-axis (left and right direction). The average speed of motion in the Y-axis left and right directions is also listed in this table.

Table 6: List of time needed for the transducer to cover different distances and average speed of motion for the Y-axis left and right directions.

Left direction				
Distance (mm)	**1**	**5**	**10**	**15**
Measurement number	**Time (s) for left motion**			
1	0.065	0.321	0.642	0.983
2	0.064	0.317	0.638	0.985
3	0.06	0.316	0.643	0.995
4	0.063	0.316	0.657	0.993
Average Time (s)	0.063	0.3175	0.645	0.989
Speed (mm/s)	15.93	14.16	14.46	14.65
Speed of left direction (average all)	14.8 mm/s			
Right direction				
Distance (mm)	**1**	**5**	**10**	**15**
Measurement number	**Time (s) for right motion**			
1	0.068	0.326	0.66	1.001
2	0.065	0.32	0.649	0.98
3	0.058	0.318	0.645	1.009

4	0.069	0.317	0.662	0.989
Average Time (s)	0.065	0.32	0.654	0.99
Speed (mm/s)	14.28	13.84	14.66	14.69
Speed of right motion (average all)	14.37 mm/s			

Evaluation of the Z-axis

The accuracy of motion in the Z-axis was assessed using the experimental set-up shown in Figure 21. The stage was moved by certain distances using the motion commands of the software, and the actual distance of the motion was recorded using the digital caliper. Again, specially designed parts were used for mounting the caliper on the motion stage under evaluation. Motion steps of 1, 5, and 10 mm were evaluated. Table 7 lists the actual measured distance at motion steps of 1, 5, and 10 mm in the Z-axis up and down directions. Figures 22 to 24 show bar charts of the measured distance for bidirectional steps of 1, 5, and 10 mm in the Z-axis, respectively, with respect to the repetition number for 20 repetitions. Accordingly, Figure 25 shows the mean values of the actual measured distance versus the intended distance for the Z-axis up and down motion.

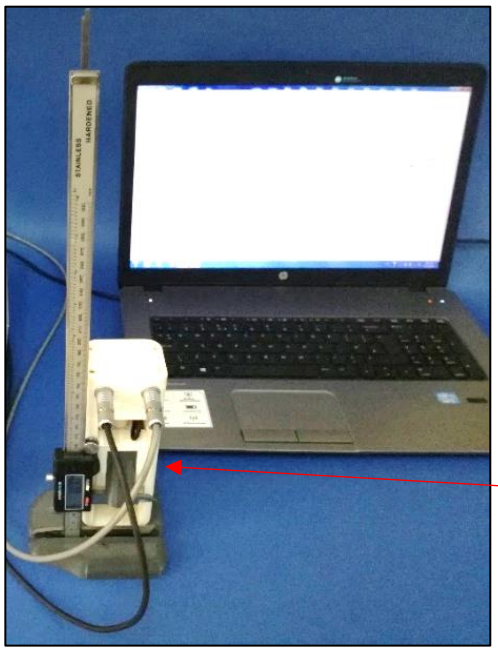

Figure 21: Evaluation of the motion of the robotic device in the Z-axis.

Table 7: List of distance measurements taken at commanded motion step of 1, 5, and 10 mm for the Z-axis evaluation.

Intended distance (mm)	**1**		**5**		**10**	
Measurement number	**Distance moved up (mm)**	**Distance moved down (mm)**	**Distance moved up (mm)**	**Distance moved down (mm)**	**Distance moved up (mm)**	**Distance moved down (mm)**
1	1.03	1.02	5.05	5.09	10.00	10.10
2	0.99	0.96	5.07	4.98	9.95	9.91
3	0.97	0.93	5.11	5.10	9.91	9.82
4	1.05	0.99	4.97	5.00	9.93	9.78
5	0.95	1.03	4.91	4.90	10.00	10.10
6	1.05	0.89	5.02	5.05	10.02	10.00
7	0.95	1.01	5.00	5.02	10.06	9.91
8	1.09	1.00	4.90	4.96	9.85	9.90
9	1.11	0.98	4.95	5.02	10.06	9.98
10	1.04	1.00	4.95	4.92	10.00	9.82
11	0.89	1.01	5.10	5.03	10.11	9.95
12	1.03	1.03	5.00	5.10	10.03	9.87
13	0.94	1.06	4.93	4.96	9.90	10.01
14	0.92	0.91	4.91	4.90	9.96	9.91
15	0.95	0.95	5.09	5.10	9.92	10.02
16	1.03	1.05	5.00	5.02	10.00	10.03
17	1.05	0.92	4.90	5.00	9.86	9.87
18	1.01	1.05	4.97	5.06	9.79	10.00
19	1.09	0.98	4.95	4.92	9.84	9.88
20	0.97	1.04	5.00	4.94	10.00	9.97
Average	**1.0055**	**0.9905**	**4.989**	**5.0035**	**9.9595**	**9.9415**
Standard deviation	**0.0596**	**0.0486**	**0.0656**	**0.0656**	**0.0816**	**0.0873**

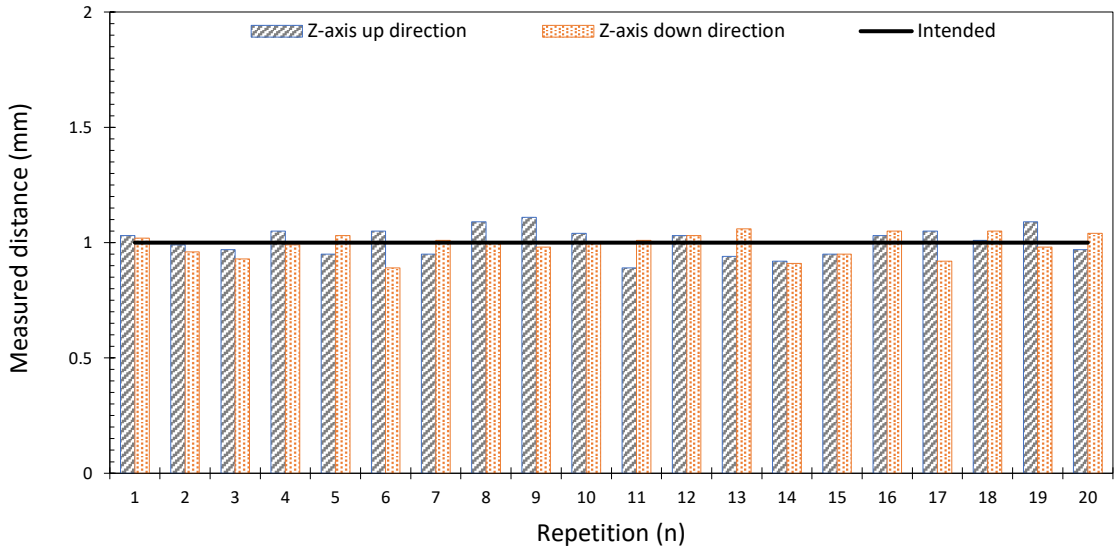

Figure 22: Distance measurements for 20 repetitions for step motion of 1 mm in the Z-axis up and down directions. The black straight line indicates the intended distance.

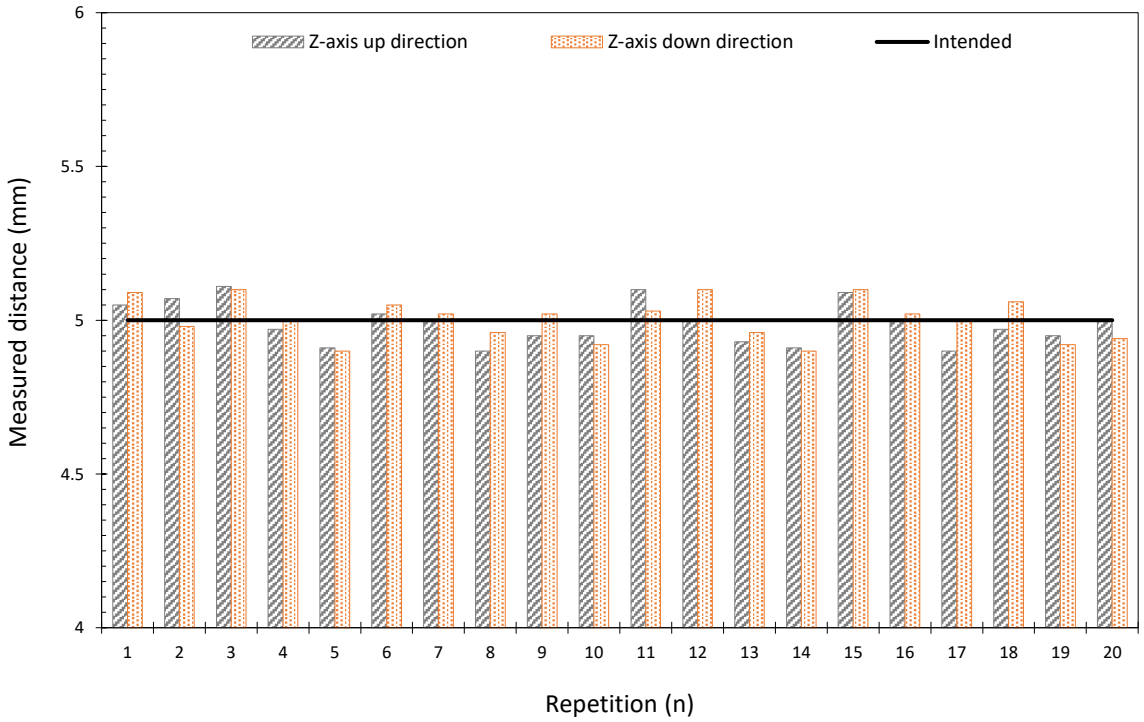

Figure 23: Distance measurements for 20 repetitions for step motion of 5 mm in the Z-axis up and down directions. The black straight line indicates the intended distance.

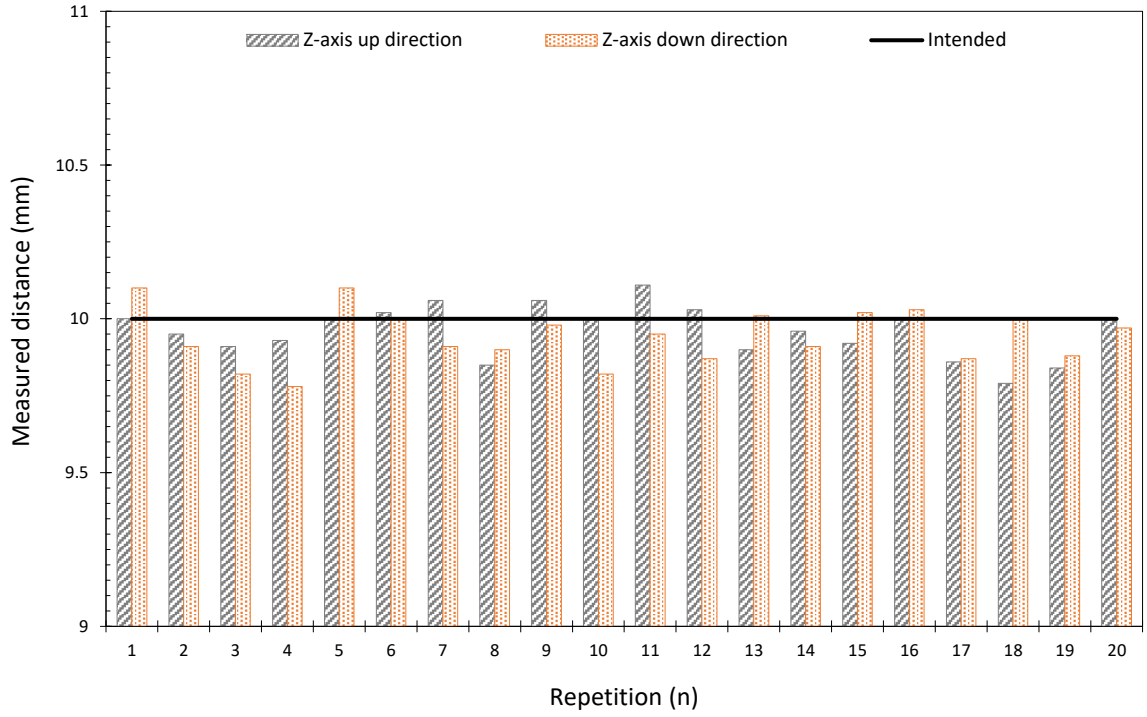

Figure 24: Distance measurements for 20 repetitions for step motion of 10 mm in the Z-axis up and down directions. The black straight line indicates the intended distance.

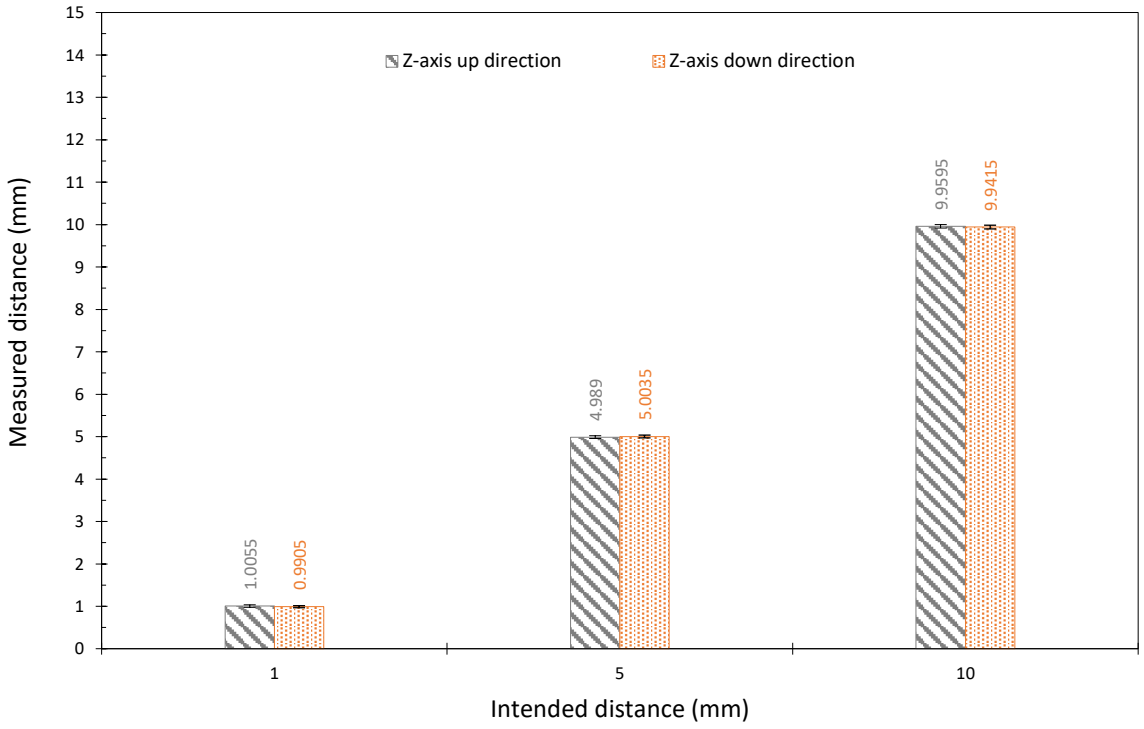

Figure 25: Mean values of the measured distance versus intended distance for the Z-axis up and down motion.

The motion error was estimated for each motion step in both Z-axis directions. Table 8 summarizes the error measured at motion steps of 1, 5, and 10 mm for the Z-axis up and down directions.

Table 8: List of error estimated at different motion steps for the Z-axis up and down directions.

Step (mm)	Error-up direction	Error-up direction (%)	Error-down direction	Error-down direction (%)
1	52	5.2	39	3.9
5	55	1.1	55	1.1
10	69	0.69	84	0.84

The speed of the motion of the robotic device in the Z-axis was also estimated. Motion steps of different distances (1, 5, 10, and 15 mm) were performed and the time needed to cover the commanded distance was calculated. Four measurements were performed for each motion step and the average speed of motion was calculated (based on the estimated average time). Table 9 lists the time needed for the transducer to cover the various distances as measured by the microcontroller, and the corresponding speed of motion for the Z-axis (up and down directions).

Table 9: List of time needed for the transducer to cover different distances and speed of motion for the Z-axis up and down directions.

Up direction				
Distance (mm)	**1**	**5**	**10**	**15**
Measurement number	**Time (s) for up direction**			
1	0.104	0.508	1.045	1.495
2	0.1	0.51	1.023	1.554
3	0.101	0.505	1.037	1.532
4	0.102	0.501	1.024	1.62
Average Time (s)	0.1018	0.506	1.032	1.55
Speed (mm/s)	9.90	9.90	9.78	9.70
Speed of up direction (average all)	9.82 mm/s			
Down direction				
Distance (mm)	**1**	**5**	**10**	**15**
Measurement number	**Time (s) for down motion**			
1	0.105	0.502	1.012	1.523
2	0.101	0.51	1.082	1.659

3	0.098	0.515	1.014	1.596
4	0.103	0.523	1.095	1.748
Average Time (s)	0.1018	0.5125	1.051	1.6315
Speed (mm/s)	10.09	9.73	9.59	9.26
Speed of down direction (average all)	9.7 mm/s			

Evaluation of the Θ-axis

The accuracy of the angular motion in the Θ-axis was also evaluated. The angular motion stage was rotated by certain degrees and the actual displacement in degrees was measured using another digital caliper (Figure 26), which can measure angles in degrees. Special 3D-printed parts were designed to hold the digital caliper in order to accurately measure angular motion. Figure 27 shows a photo of the experimental set-up with the electronic driving system and the software. Angle steps of 1, 5, and 10^{o} were evaluated. Table 10 lists the actual measured angles at commanded angle steps of 1, 5, and 10^{o} about the Θ-axis. Figures 28 to 30 show bar charts of the measured angle for bidirectional angle steps of 1, 5, and 10^{o} about the Θ-axis, respectively, with respect to the repetition number for 20 repetitions. Accordingly, Figure 31 shows the mean value of the actual measured angle versus the intended angle for the Θ-axis CW and CCW motion.

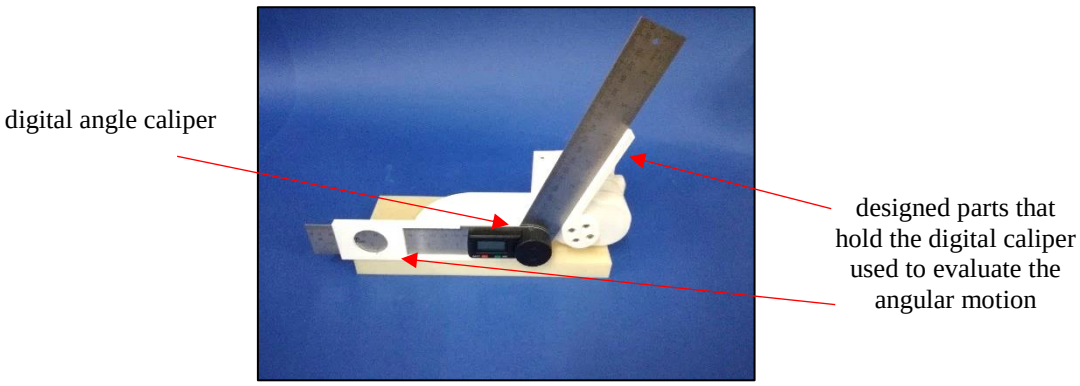

Figure 26: The digital caliper and specially designed parts that were used to evaluate the angular motion of the robotic system.

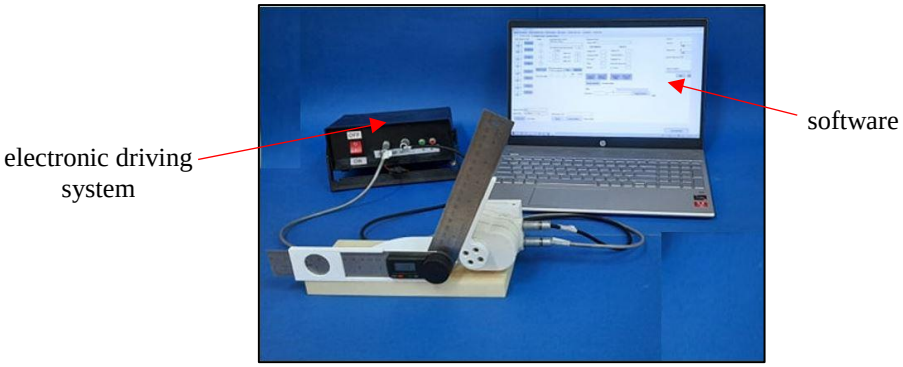

Figure 27: Experimental set-up for evaluation of the angular motion (Θ-axis) of the robotic device.

Table 10: List of angle measurements taken at commanded angle step of 1, 5, and 10 degrees for the Θ-axis evaluation.

Intended angle (degrees)	**1**		**5**		**10**	
Measurement number	**CW Angle (degrees)**	**CCW Angle (degrees)**	**CW Angle (degrees)**	**CCW Angle (degrees)**	**CW Angle (degrees)**	**CCW Angle (degrees)**
1	1.1	1.2	4.8	4.7	10.1	10.0
2	0.9	1.3	4.9	5.0	10.4	10.5
3	1.0	1.2	5.5	5.6	10.7	10.6
4	1.0	1.3	5.0	4.7	10.3	10.0
5	0.9	1.0	5.7	5.6	10.6	10.7
6	0.8	1.3	5.1	5.3	10.1	10.2
7	1.2	1.2	5.2	5.0	10.7	10.2
8	1.2	1.1	5.4	5.6	10.4	10.0
9	1.2	1.3	5.4	5.0	10.1	10.0
10	1.1	1.1	5.3	5.4	10.6	10.4
11	0.9	1.2	4.8	4.9	9.9	10.0
12	1.0	1.1	5.1	5.0	10.4	10.3
13	1.1	0.9	5.2	5.4	10.5	10.6
14	1.0	1.0	4.8	4.9	9.9	10.2
15	0.8	0.9	5.5	5.2	10.6	10.5
16	0.9	0.8	5.2	5.1	10.1	10.0
17	1.0	1.0	5.1	5.2	10.1	10.6
18	1.0	0.8	5.4	5.3	9.9	10.5
19	1.2	0.9	4.9	5.2	9.9	10
20	1.1	0.9	5.1	5.2	10.3	10.5
Average	**1.02**	**1.075**	**5.17**	**5.165**	**10.28**	**10.29**
Stand. deviation	**0.1249**	**0.1670**	**0.2532**	**0.2651**	**0.2731**	**0.2508**

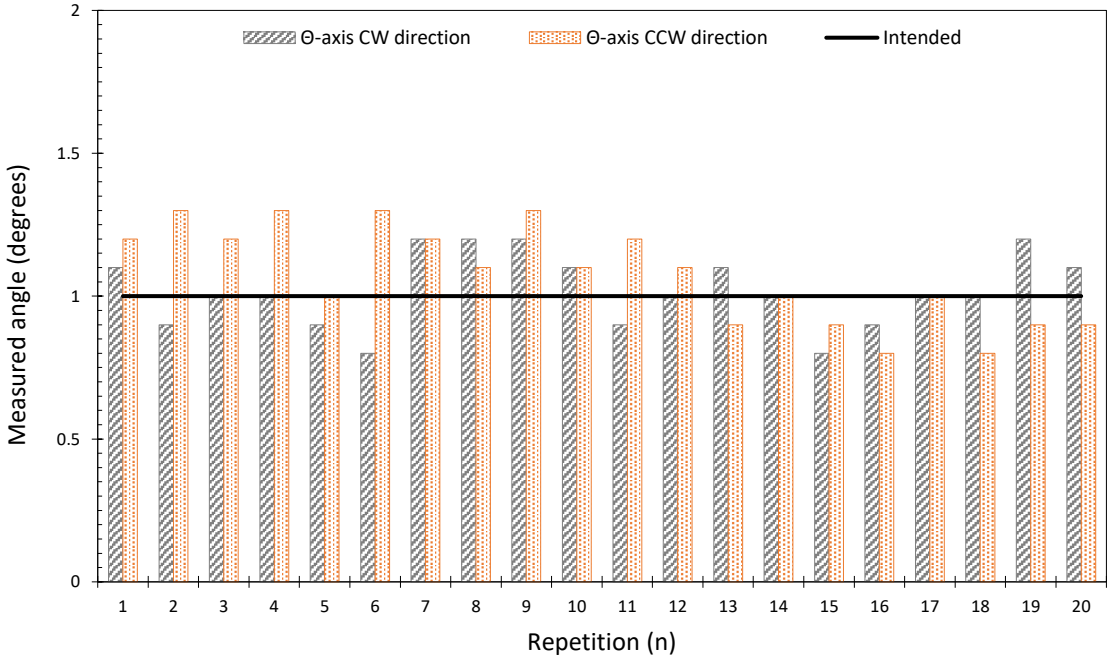

Figure 28: Angle measurements for 20 repetitions for angle step of 1° in the Θ-axis CW and CCW directions. The black straight line indicates the intended distance.

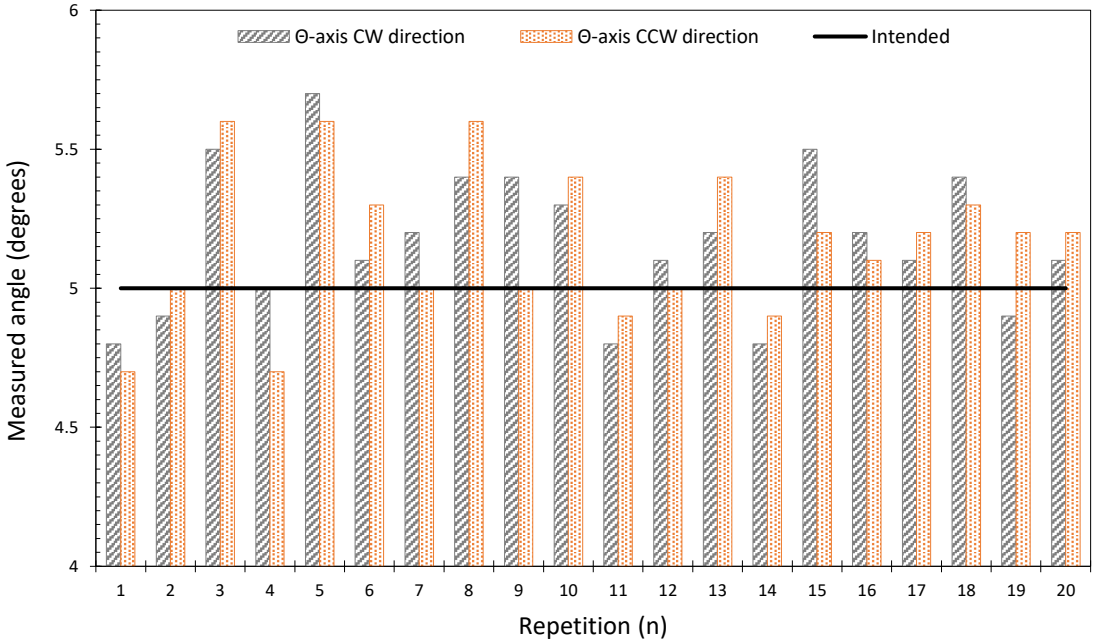

Figure 29: Angle measurements for 20 repetitions for angle step of 5° in the Θ-axis CW and CCW directions. The black straight line indicates the intended distance.

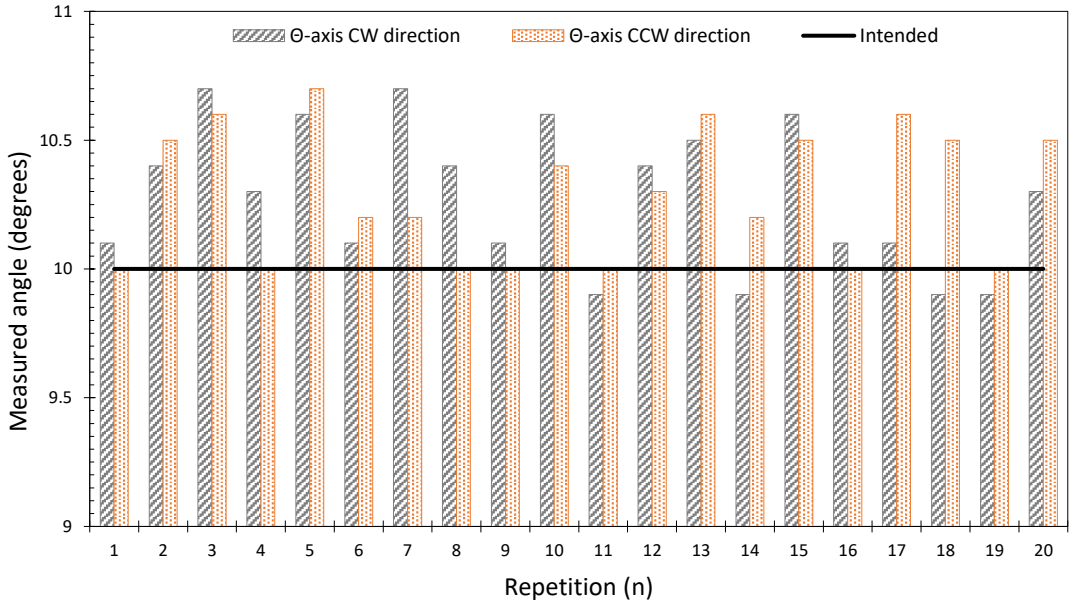

Figure 30: Angle measurements for 20 repetitions for angle step of 10^{o} in the Θ-axis CW and CCW directions. The black straight line indicates the intended distance.

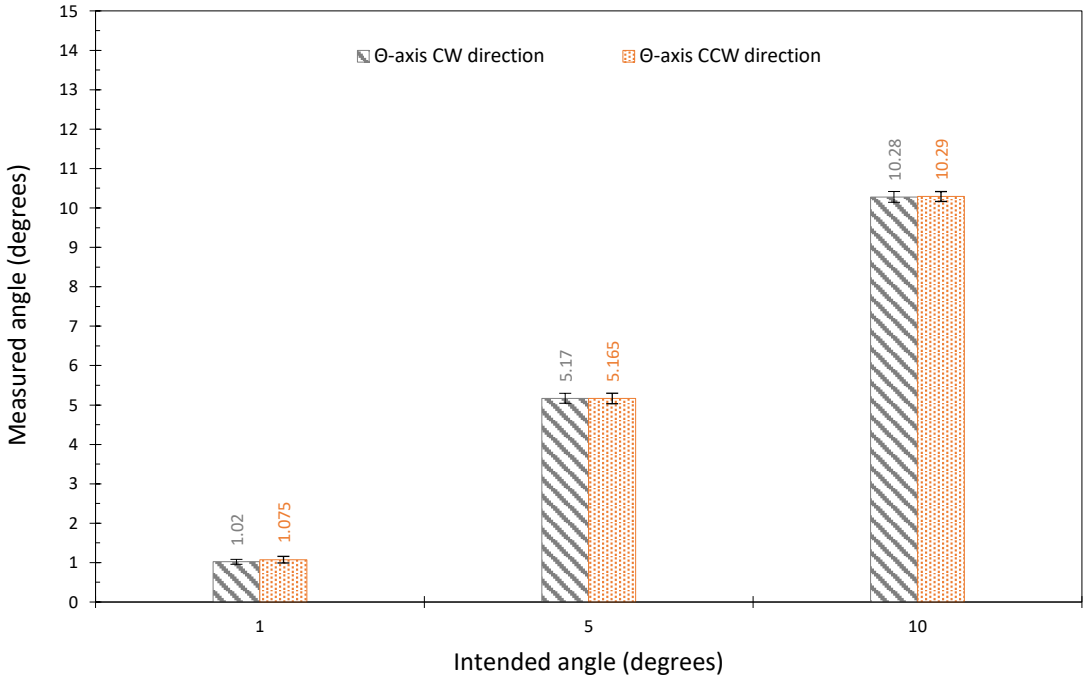

Figure 31: Mean value of the measured angle versus intended angle for the Θ-axis CW and CCW motion.

The motion error was estimated for each angle step about both Θ-axis directions. Table 11 summarizes the error value (in degrees and percentage) measured at angle steps of 1, 5, and 10^{o} for the Θ-axis CW and CCW directions.

Table 11: List of error estimated at different angle steps for the Θ-axis CW and CCW directions.

Step (degrees)	Error-CW motion (degrees)	Error-CW motion (%)	Error-CCW motion (degrees)	Error-CCW motion (%)
1	0.1	10	0.155	15.5
5	0.25	5	0.245	4.9
10	0.32	3.2	0.29	2.9

The speed of the angular motion of the robotic device was also estimated. The average speed for angle steps of 1, 5, 10, and 15^{o} was calculated. Table 12 lists the time needed for the transducer to rotate by various degrees, and the corresponding speed of angular motion (CW and CCW direction).

Table 12: List of time needed for the transducer to rotate by various degrees and speed of CW and CCW angular motion.

Forward direction				
Angle (degrees)	**1**	**5**	**10**	**15**
Measurement number	**Time (s) for CW angular motion**			
1	0.01	0.038	0.072	0.104
2	0.009	0.035	0.069	0.101
3	0.008	0.035	0.069	0.103
4	0.008	0.033	0.071	0.106
Average Time (s)	0.0088	0.03525	0.07	0.1035
Speed (º/s)	132.43	144.5	148.42	147.65
Speed of CW motion (average all)	143.25 º/s			
Reverse direction				
Angle (degrees)	**1**	**5**	**10**	**15**
Measurement number	**Time (s) for CCW angular motion**			
1	0.009	0.034	0.069	0.104
2	0.008	0.036	0.068	0.101
3	0.011	0.034	0.068	0.106
4	0.01	0.04	0.072	0.105
Average Time (s)	0.0095	0.036	0.069	0.104
Speed (º/s)	118.78	145.13	144.46	146.21
Speed of CCW motion (average all)	138.64 º/s			

Evaluation of the robotic system version 2

Four DOF robotic system version 2

The motion accuracy of the robotic system version 2 was evaluated in the X and Y axes using digital calipers. The robotic system comprises four motion stages as the previous version, but larger piezoelectric motors (USR60-S3N, Shinsei Corporation, Kasuya Setagaya-ku, Tokyo, Japan) and dual digital encoders (with the appropriate strip for each encoder). The CAD drawing of the fully assembled 4 DOF robotic device version 2 is shown in Figure 32. The direction of each motion axis of the device is indicated (Figure 32a). All the components, which have been assembled to develop the robotic system, are described in detail in Deliverable 3.1 (Four DOF robotic system-version 2).

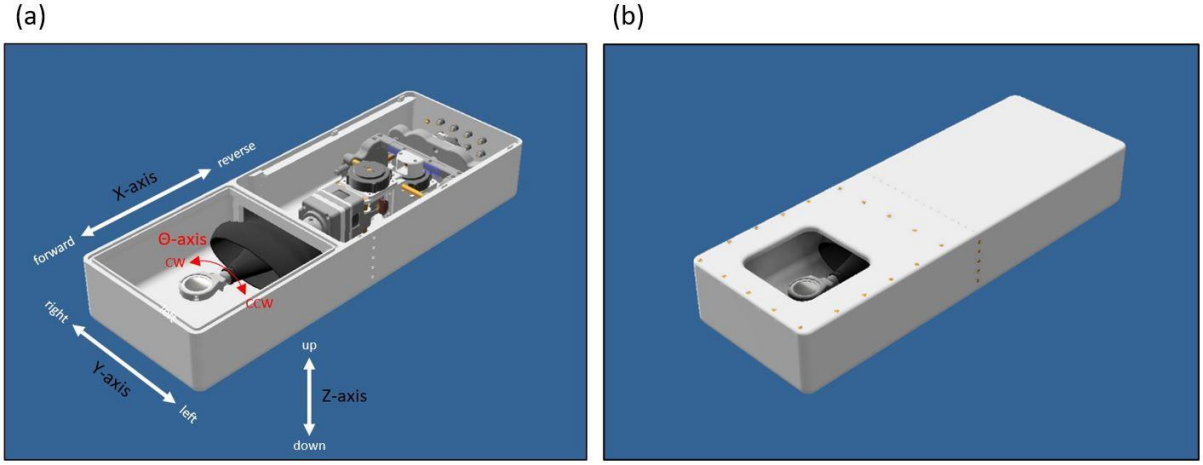

Figure 32: CAD drawing of the 4 DOF robotic system version 2 a) without the cover, and b) with the cover.

Every motion stage of the robotic device is PC-controlled through the designed software. Due to the constraints of the MRI bore, there are some spatial limits. The maximum distance the transducer holder can move, from the one end to the other, is 60 mm in the X-axis, 75 mm in the Y-axis, and 26 mm in the Z-axis. The rotation limit is 90 degrees (45 degrees CW and 45 degrees CCW).

Electronic system

The electronic system that is responsible to control the large motors is composed of a digital acquisition (DAQ) card, motor encoders, and a power supply. The electronic system is described in detail in Deliverable 3.3 (Electronic driving system) and a photo is shown in Figure 33.

Figure 33: Electronic system of the robotic system version 2.

Evaluation of the X-axis

The accuracy of the motion of the X-axis was evaluated using a digital caliper and additional 3D-printed parts. Figure 34 shows the CAD drawing of the parts that were designed for mounting the caliper on the device to accurately evaluate the X-axis motion of the robotic system.

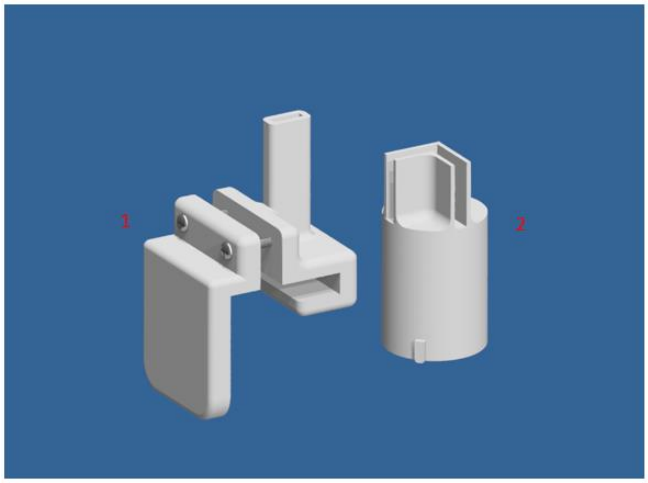

Figure 34: CAD drawings of the parts that were used to evaluate the X-axis motion of the robotic device.

Figure 35 shows the CAD drawing of the set-up that was used to estimate the accuracy of the X-axis motion attached to the robotic device.

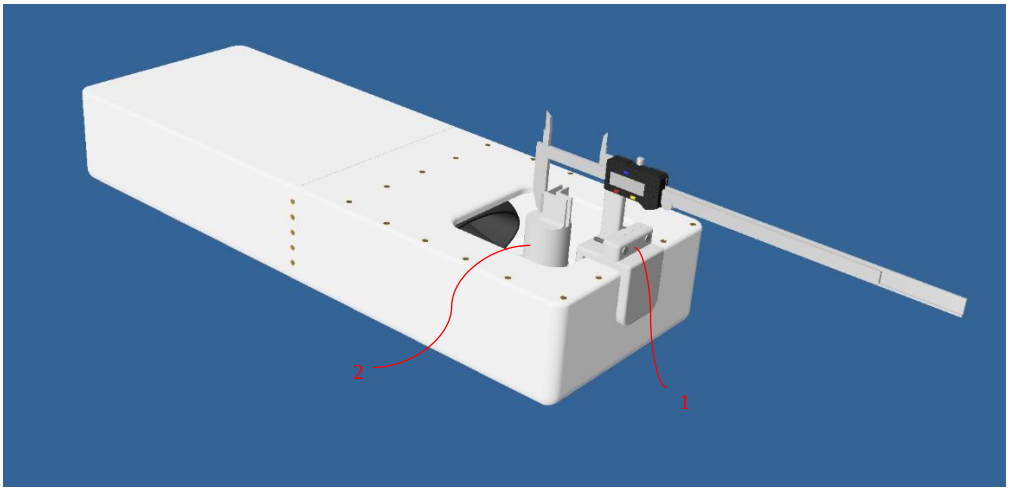

Figure 35: CAD drawing of the set-up that was used to estimate the accuracy of the X-axis motion.

Table 13 lists the actual measured distance at commanded motion steps of 1, 5, and 10 mm in the X-axis. Figures 36 to 38 show bar charts of the measured distance for bidirectional motion steps of 1, 5, and 10 mm in the X-axis, respectively, with respect to the repetition number for 20 repetitions. Accordingly, Figure 39 shows the mean value of the actual measured distance versus the intended distance for the X-axis forward and reverse motion.

Table 13: List of distance measurements taken at commanded motion step of 1, 5, and 10 mm for the X-axis evaluation.

Intended distance (mm)	**1**		**5**		**10**	
Measurement number	**Distance moved forward (mm)**	**Distance moved reverse (mm)**	**Distance moved forward (mm)**	**Distance moved reverse (mm)**	**Distance moved forward (mm)**	**Distance moved reverse (mm)**
1	1	0.99	5.03	5.15	10.05	10
2	0.98	1.03	4.94	5.04	10.13	10.19
3	0.88	1.08	4.89	4.9	10.04	9.97
4	1.02	0.99	4.95	5.03	10.09	10
5	0.97	1.01	4.92	4.93	10.16	9.82
6	0.88	1.05	5.02	5.05	10.06	10.02
7	1.03	1.03	4.88	4.9	10.08	10.16
8	1.01	0.9	4.96	4.98	9.92	9.93
9	1.04	0.89	5.01	4.91	10.03	9.94
10	0.98	0.98	4.95	5.11	9.99	10.01
11	1.06	1.03	5.01	5.05	10	10.03
12	0.97	1.06	4.97	5	9.94	9.99
13	0.99	0.93	4.92	5.01	10.02	10.05

14	0.93	0.92	5.01	4.97	9.96	10.02
15	0.97	0.95	5.06	4.95	10.18	10
16	1.02	1.02	5	4.96	10.08	10.09
17	0.94	0.97	4.94	4.88	10.07	9.94
18	0.95	0.91	4.97	4.85	9.78	10.04
19	1.03	0.96	4.92	4.94	10.15	10.08
20	0.94	0.9	4.99	4.98	10.06	10.06
Average	**0.980**	**0.980**	**4.967**	**4.980**	**10.040**	**10.017**
Standard deviation	**0.048**	**0.057**	**0.047**	**0.075**	**0.091**	**0.079**

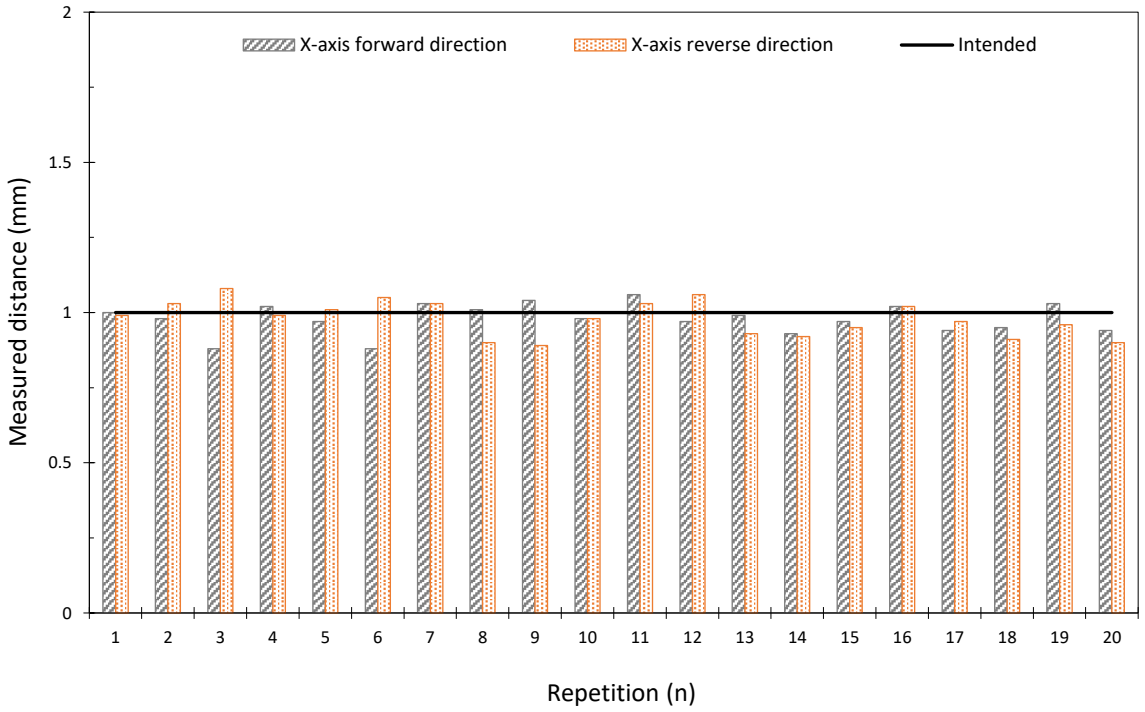

Figure 36: Distance measurements for 20 repetitions for step motion of 1 mm in the X-axis forward and reverse directions. The black straight line indicates the intended distance.

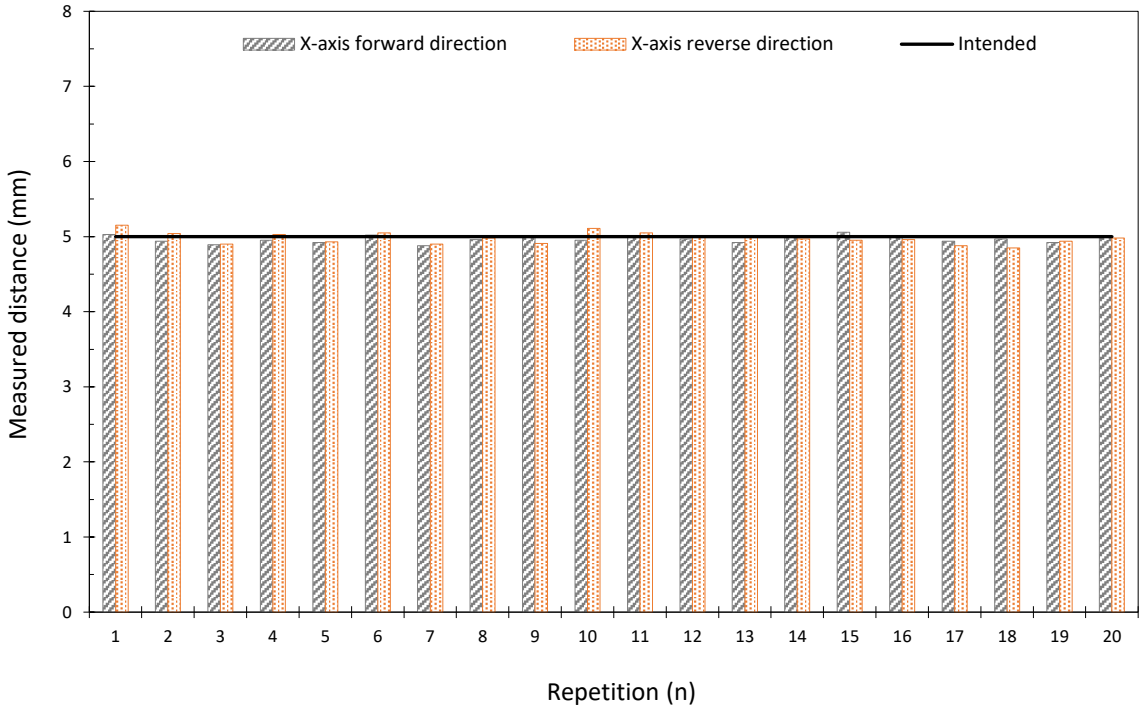

Figure 37: Distance measurements for 20 repetitions for step motion of 5 mm in the X-axis forward and reverse directions. The black straight line indicates the intended distance.

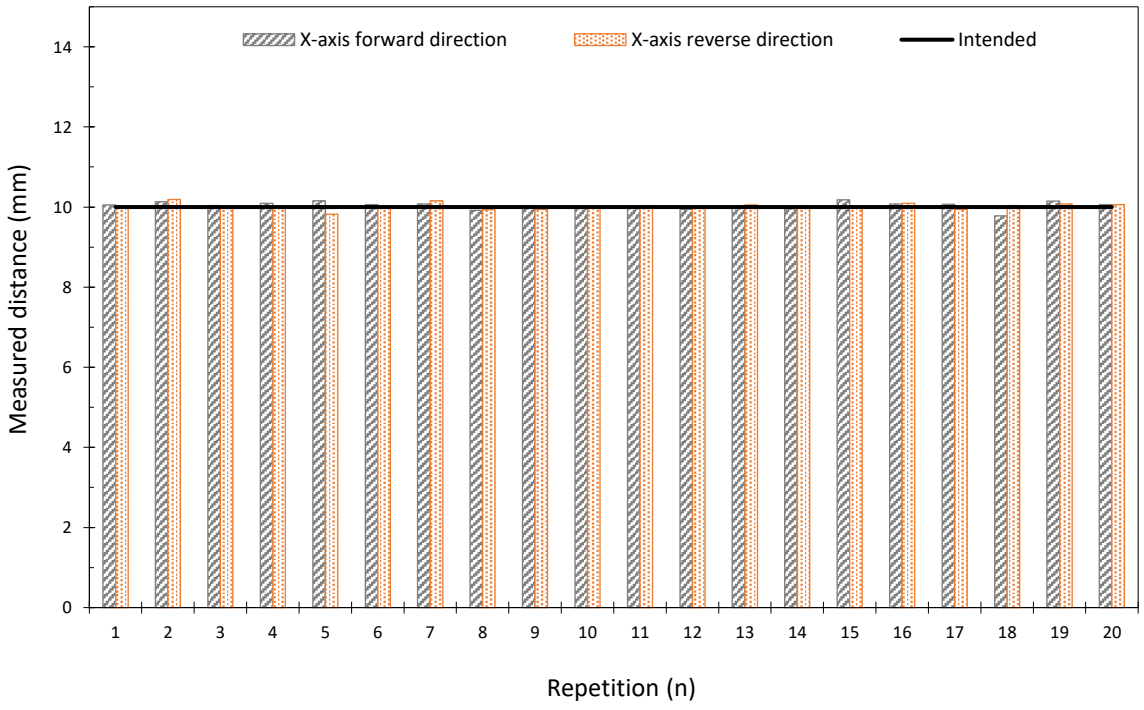

Figure 38: Distance measurements for 20 repetitions for step motion of 10 mm in the X-axis forward and reverse direction. The black straight line indicates the intended distance.

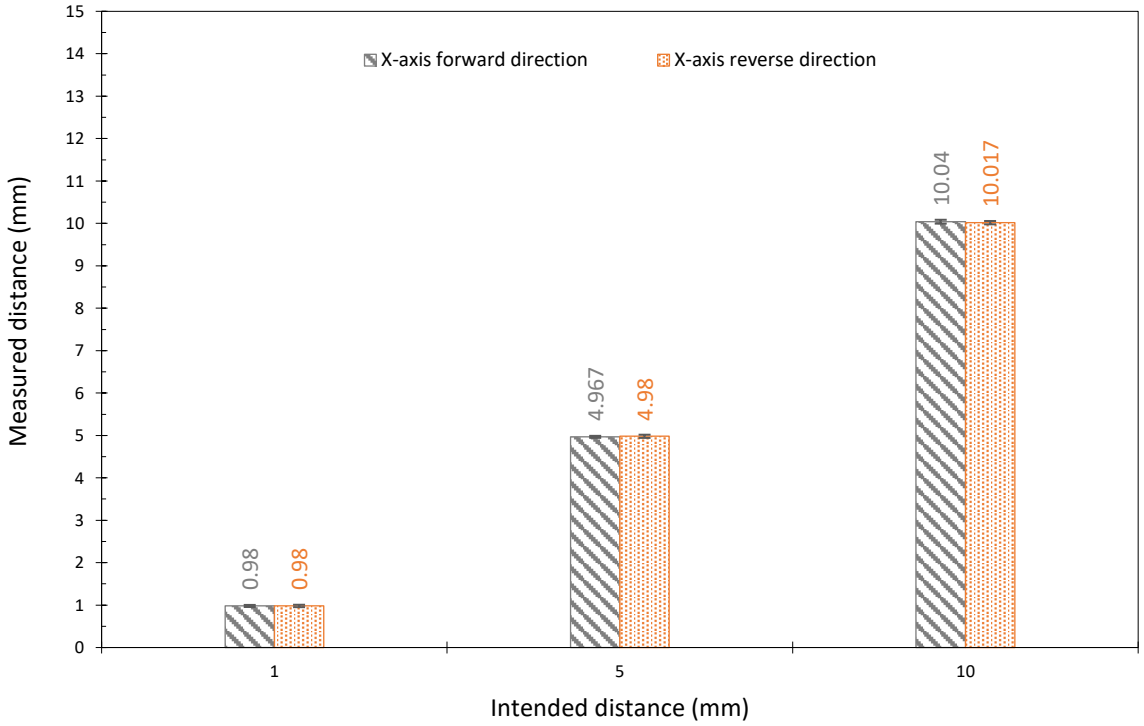

Figure 39: Mean value of the measured distance versus intended distance for the X-axis forward and reverse motions.

The motion error was estimated for each motion step in both X-axis directions. Table 14 summarizes the error measured at motion steps of 1, 5, and 10 mm for the X-axis forward and reverse directions.

Table 14: List of error estimated at different motion steps for the X-axis forward and reverse directions.

Step (mm)	Error-forward motion (µm)	Error-forward motion (%)	Error-reverse motion (µm)	Error-reverse motion (%)
1	42	4.2	51	5.1
5	47	0.94	65	1.3
10	81	0.81	58	0.58

Evaluation of the Y-axis

The accuracy of the motion of the Y-axis was also evaluated using the digital caliper. Table 15 lists the actual measured distance at motion steps of 1, 5, and 10 mm in the Y-axis. Figures 40 to 42 show bar charts of the measured distance for bidirectional motion steps of 1, 5, and 10 mm in the Y-axis, respectively, with respect to the repetition number for 20 repetitions.

Accordingly, Figure 43 shows the mean value of the actual measured distance versus the intended distance for the Y-axis left and right motion.

Table 15: List of distance measurements taken at motion steps of 1, 5, and 10 mm for the Y-axis evaluation.

Intended distance (mm)	**1**		**5**		**10**	
Measurement number	**Distance moved left (mm)**	**Distance moved right (mm)**	**Distance moved left (mm)**	**Distance moved right (mm)**	**Distance moved left (mm)**	**Distance moved right (mm)**
1	1.03	0.98	5.07	4.96	10.18	9.86
2	1.09	1.07	4.94	4.97	10.09	9.98
3	0.97	0.98	5.01	5.09	9.85	9.97
4	1.04	1.09	5.09	5.04	9.95	10.18
5	1.01	1.04	4.99	5.08	10.03	10.26
6	1.03	0.97	5.17	5	10.18	9.93
7	0.94	0.89	5.05	5.05	10.06	9.9
8	0.98	1.01	5.19	5.11	10.08	10.2
9	0.99	1.02	4.98	5.06	9.96	10.14
10	0.95	1	5.1	5.05	10.01	10.02
11	0.98	0.99	4.92	4.89	10.14	9.87
12	0.96	0.99	5.15	5	9.99	9.89
13	1.05	0.89	4.9	4.95	9.95	10.03
14	0.96	1.02	5.11	5.07	10.11	10.08
15	1.01	1	5.1	5.03	10.04	10.29
16	0.92	0.88	5.07	5.02	10.23	9.86
17	0.96	0.93	5.14	5.07	10.06	9.96
18	0.97	0.99	5.08	5.09	9.99	10.05
19	0.89	0.88	5.02	4.96	9.91	10.16
20	1.04	0.98	5.06	5.02	10.11	10.26
Average	**0.989**	**0.980**	**5.057**	**5.026**	**10.046**	**10.045**
Standard deviation	**0.048**	**0.058**	**0.079**	**0.056**	**0.095**	**0.140**

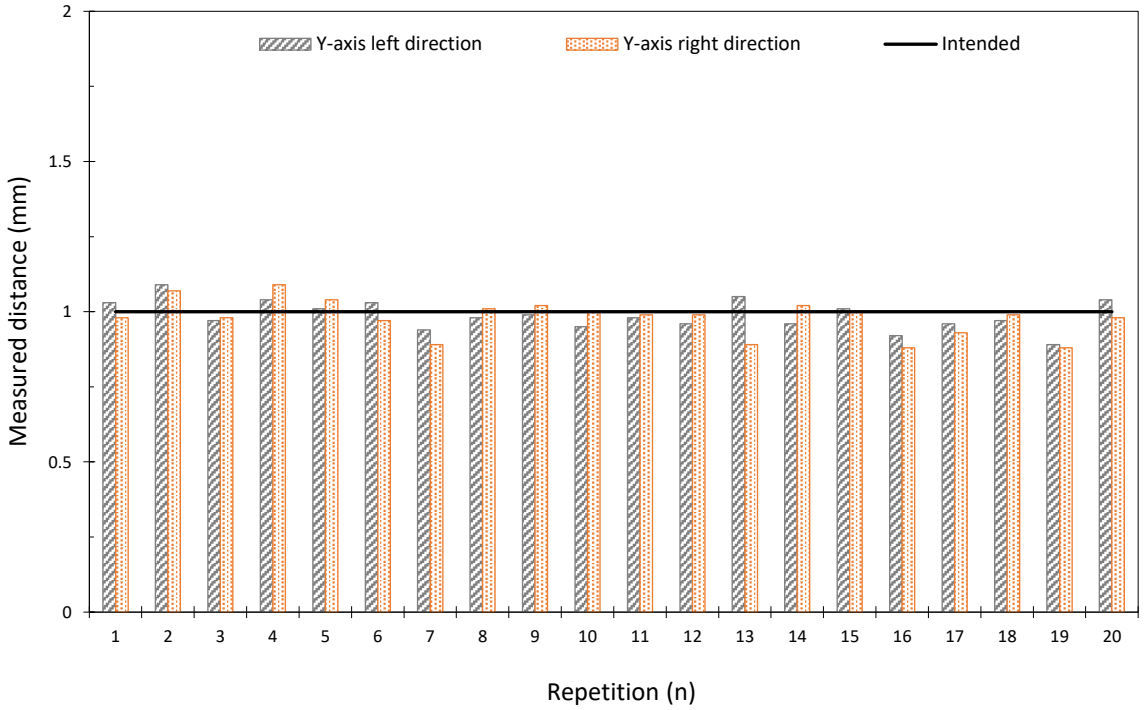

Figure 40: Distance measurements for 20 repetitions for step motion of 1 mm in the Y-axis left and right directions. The black straight line indicates the intended distance.

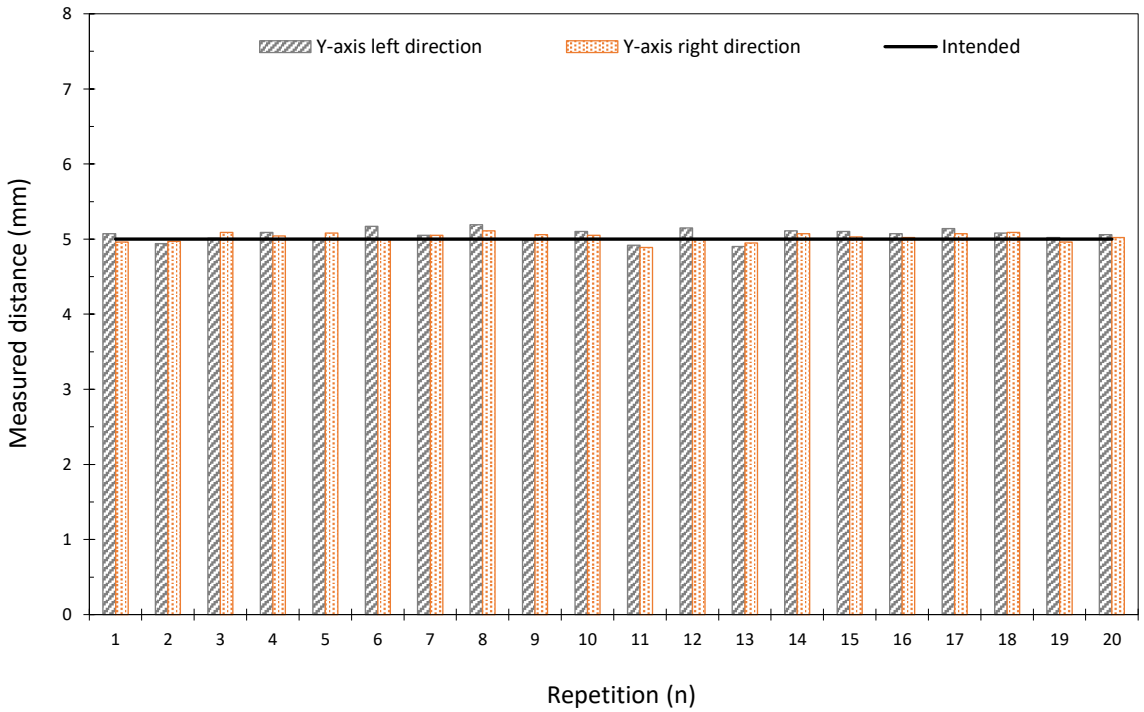

Figure 41: Distance measurements for 20 repetitions for step motion of 5 mm in the Y-axis left and right direction. The black straight line indicates the intended distance.

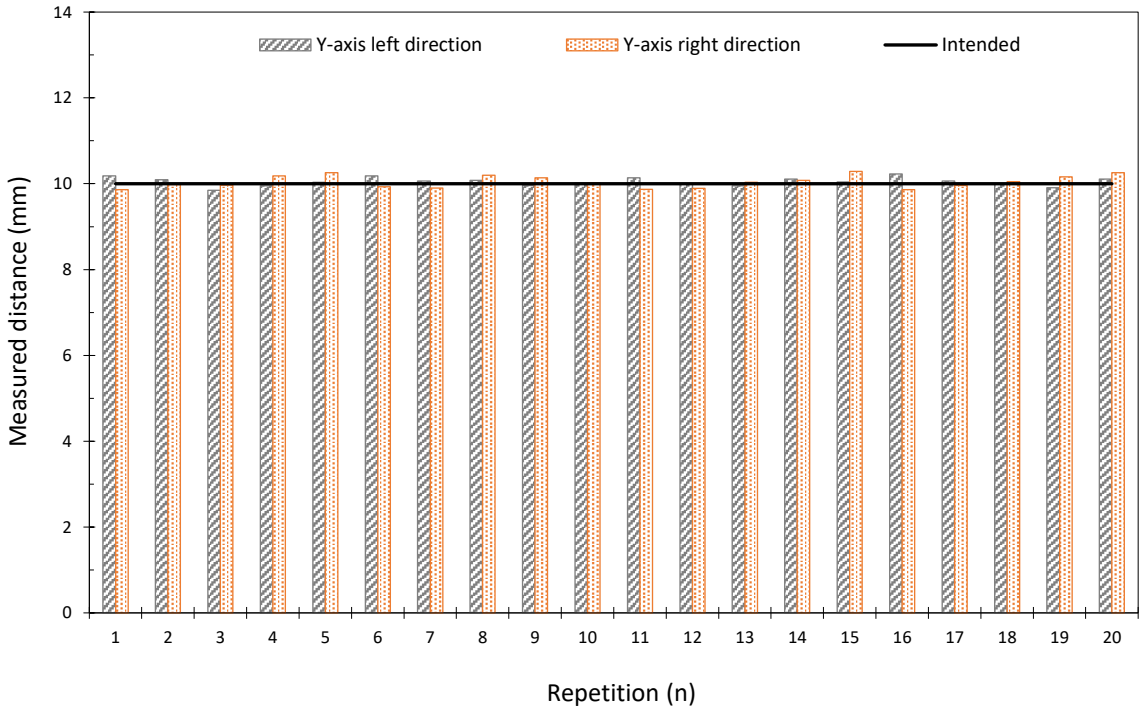

Figure 42: Distance measurements for 20 repetitions for step motion of 10 mm in the Y-axis left and right directions. The black straight line indicates the intended distance.

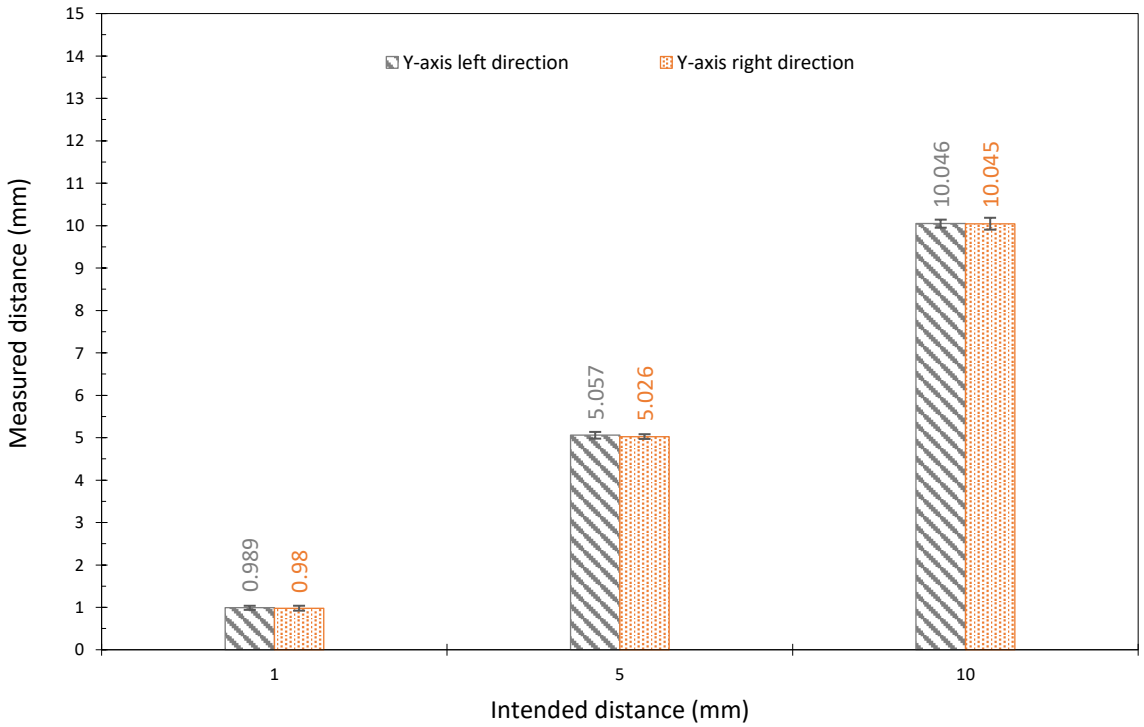

Figure 43: Mean value of the measured distance versus intended distance for the Y-axis left and right motions.

The motion error was estimated for each motion step in both Y-axis directions. Table 16 summarizes the error measured at motion steps of 1, 5, and 10 mm for the Y-axis left and right directions.

Table 16: List of error estimated at different motion steps for the Y-axis left and right directions.

Step (mm)	Error-left motion (µm)	Error-left motion (%)	Error-right motion (µm)	Error-right motion (%)
1	42	4.2	45	4.5
5	84	1.68	53	1.06
10	86	0.86	123	1.23

Evaluation of the motion accuracy using MRI

The motion accuracy of the robotic device version 2 was evaluated using MRI. The accuracy of linear motion was assessed in two axes, X and Y. The concept of the proposed technique was based on the fact that structures without protons appear dark in MR images. The focused transducer was replaced with a 3D-printed plastic structure with a tip of 2 mm thickness, which served as a marker in the MR images, and the water enclosure was filled with degassed water. The robotic device was placed inside an MRI scanner (1.5 T, GE Signa HD16, General Electric Healthcare, Chicago, Illinois, United States) and covered with a general-purpose flex surface coil (Signa 1.5 T, General Electric Medical Systems, Milwaukee, Wisconsin, USA). Figure 44a illustrates the experimental setup as placed on the MRI table, while Figure 44b shows a CAD drawing of the plastic marker. MR scanning was performed using a FSE sequence in coronal plane. The main MRI parameters were: repetition time (TR) = 800 ms, echo time (TE) = 19 ms, flip angle = 90^{o}, echo train length (ETL) = 3, pixel bandwidth = 66.1, and field of view (FOV) = 280 x 280 x 10 mm^{3}. The initial position of the tip was located, and then the transducer was moved by a certain distance. Bidirectional movements with step of 3 and 5 mm in both X and Y axes were tested. An MR image was acquired after each step movement to detect the tip location. A special approach was followed for locating the 2 mm thick tip of the plastic marker and estimating its position. First, the image zoom was enhanced to focus on the plastic marker. Then, the corresponding pixels were scanned to identify the x and y coordinates of the pixel with the lowest signal intensity (this was assumed to be the centre of the marker in the image). The change in pixel number after a step movement reflected the shift in position of the transducer in the tested direction. Therefore, the pixel difference was multiplied by the pixel

size (0.5469 mm) of the acquisition to estimate the shift in mm. This technique had an inherent error of ±1 pixel, which translated to ± 0.5469 mm. Finally, the series of images were superimposed onto one image for visualizing the motion patterns.

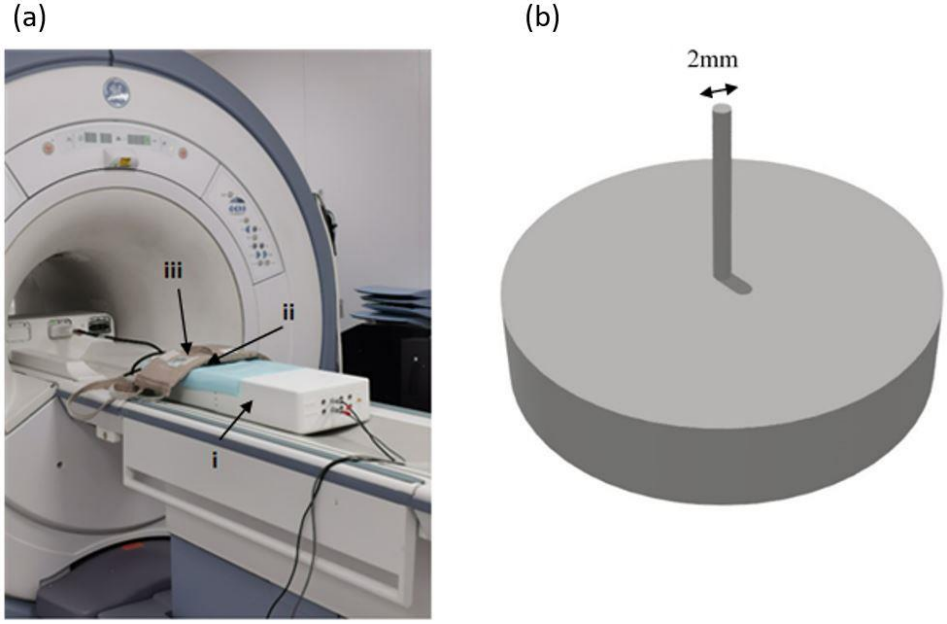

Figure 44: a) The robotic device (i) as placed on the MRI table, showing the location of the plastic marker (ii) and the flex surface coil (iii), b) CAD drawing of the plastic marker.

Evaluation of the X-axis

The robotic system was moved with motion steps of 3 and 5 mm in the X-axis and an MR FSE image was acquired after each step. Figure 45 shows indicative results for the 3-mm motion step.

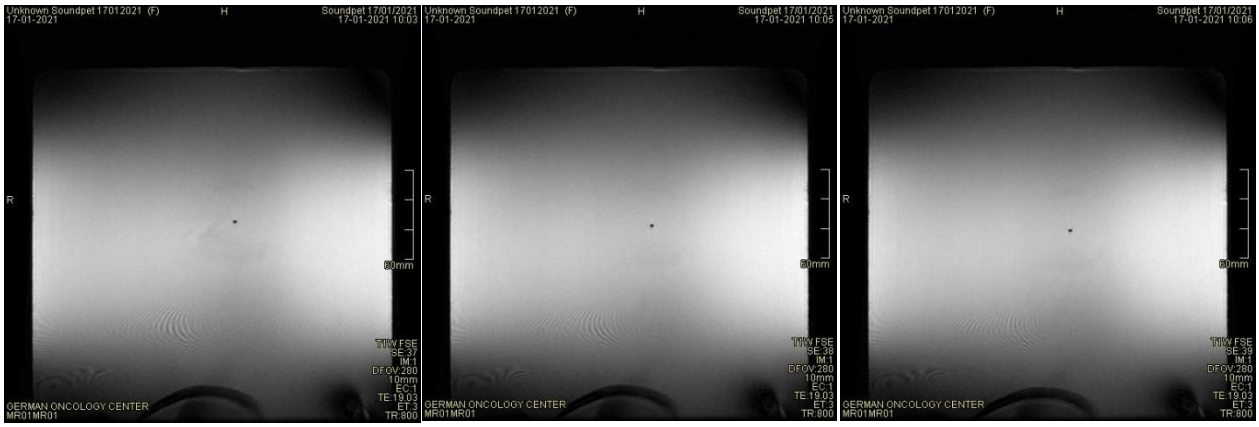

Figure 45: FSE images showing the tip location after 3-mm motion steps in the X-axis.

The acquired MR images were superimposed onto the image shown in Figure 46.

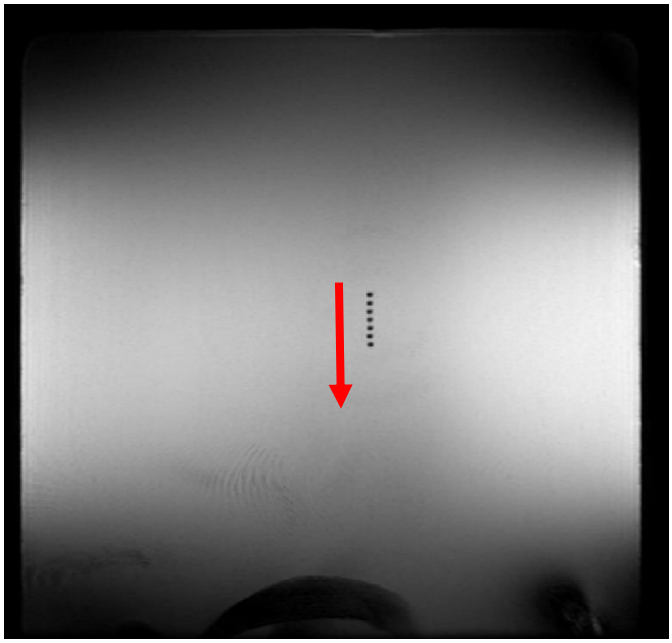

Figure 46: Minimum Intensity Projection from a combination of images that indicates motion in the X-axis reverse direction (3-mm motion step).

Table 17 lists the actual distance as calculated from the MR images at commanded motion steps of 3 and 5 mm in the X-axis forward and reverse directions. Figures 47 and 48 show bar charts of the measured distance for bidirectional motion steps of 5 and 3 mm in the X-axis, respectively, with respect to the repetition number for 10 repetitions. Figure 49 shows the mean value of the actual measured distance versus the intended distance for the X-axis forward and reverse motion.

Table 17: List of distance measurements taken at motion step of 5 and 3 mm for the X-axis evaluation.

Intended distance (mm)	**5**		**3**	
Measurement Number	**Distance moved forward (mm)**	**Distance moved reverse (mm)**	**Distance moved forward (mm)**	**Distance moved reverse (mm)**
1	5.469	4.9221	3.2814	3.2814
2	5.469	4.9221	2.7345	3.2814
3	5.469	4.9221	3.2814	3.2814
4	5.469	5.469	3.2814	3.2814
5	5.469	5.469	2.7345	3.2814
6	4.9221	5.469	3.2814	3.2814
7	5.469	5.469	3.2814	3.2814
8	4.9221	5.469	2.7345	3.2814
9	4.9221	5.469	3.2814	3.8283

10	-	5.469	3.2814	-
Average	**5.2867**	**5.3049**	**3.1173**	**3.3421**
Standard deviation	**0.2735**	**0.2641**	**0.2641**	**0.1823**

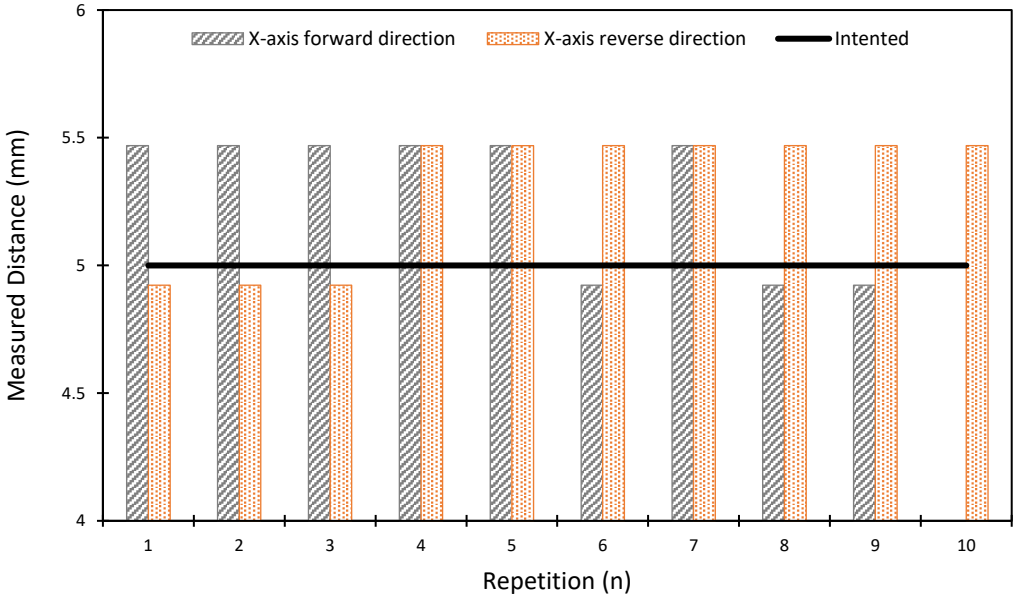

Figure 47: Distance measurements for 10 repetitions for movement step of 5 mm in the X-axis forward and reverse directions. The black straight line indicates the intended distance.

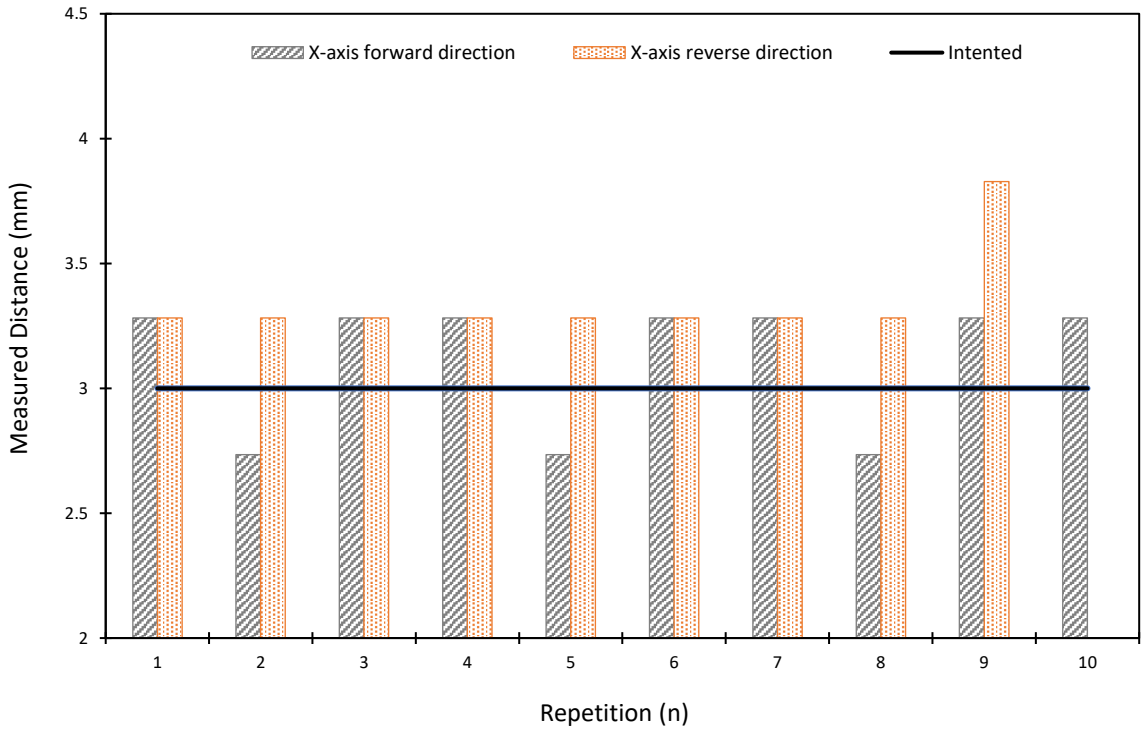

Figure 48: Distance measurements for 10 repetitions for movement step of 3 mm in the X-axis forward and reverse directions. The black straight line indicates the intended distance.

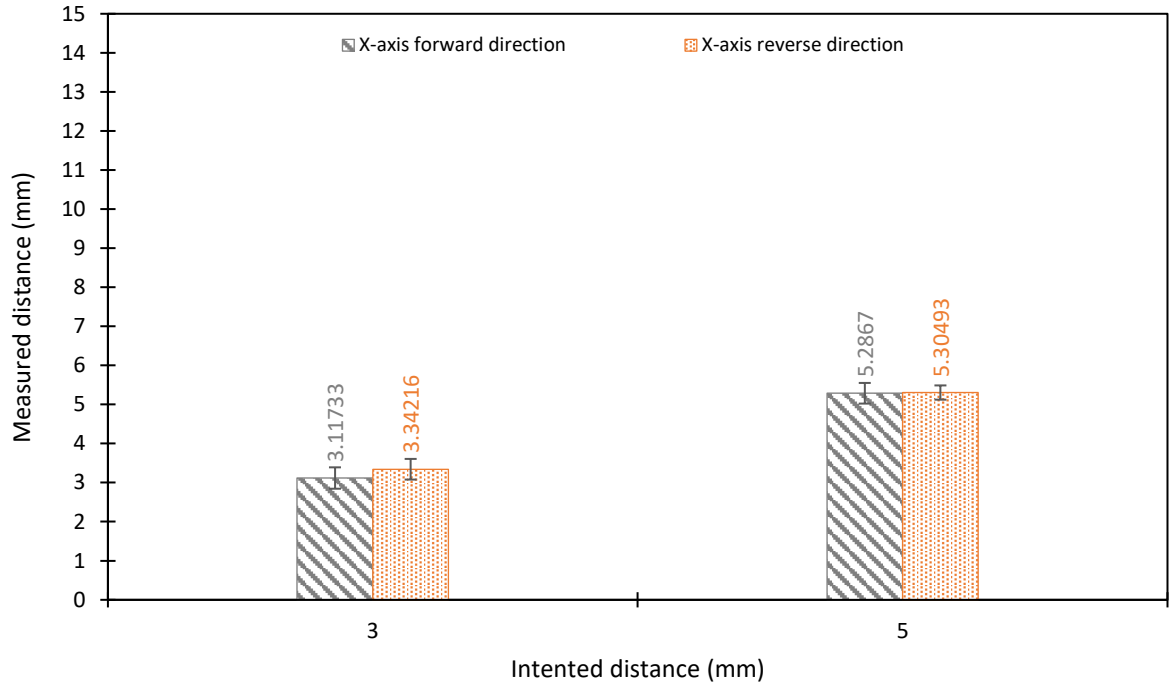

Figure 49: Mean value of the measured distance versus intended distance for the X-axis forward and reverse motions. Error bars correspond to the standard deviation.

The motion error was estimated for each motion step in both X-axis directions.. Table 18 summarizes the error measured at motion steps of 5 and 3 mm for the X-axis forward and reverse directions.

Table 28: List of error estimated at different motion steps for the X-axis forward and reverse directions.

Step (mm)	Error-forward motion (μm)	Error-forward motion (%)	Error-reverse motion (μm)	Error-reverse motion (%)
5	286.7	5.73	304.93	6.10
3	117.33	3.91	342.17	11.41

Evaluation of the Y-axis

Similarly, the robotic system was moved with specific motion steps in the Y-axis and an MR FSE image was acquired after each motion step. Figure 50 shows indicative results for the 3-mm motion step.

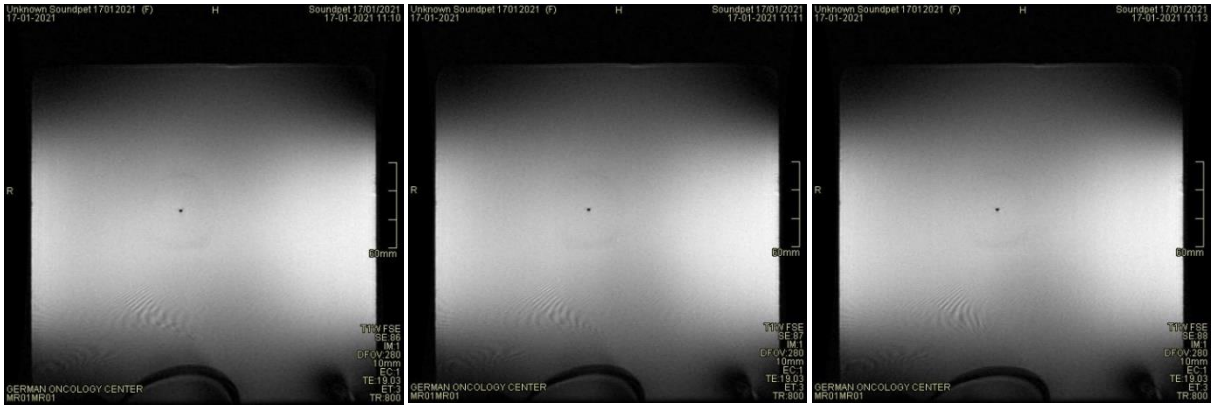

Figure 50: FSE images showing the tip location after 3-mm motion steps in the Y-axis

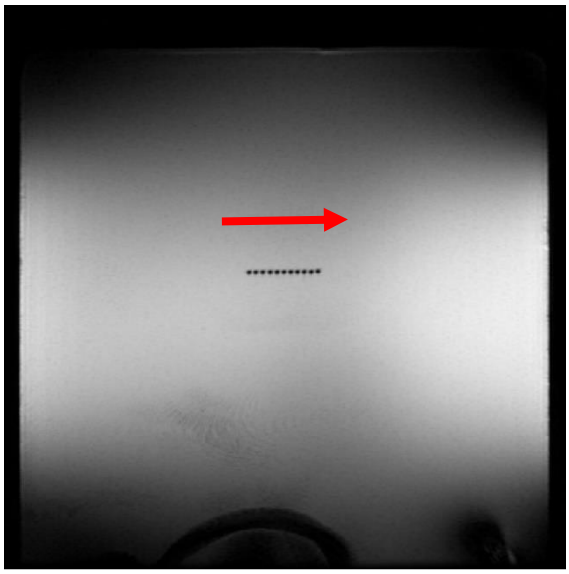

Figure 51: Minimum Intensity Projection from a combination of images that indicates motion in the Y-axis right direction (3-mm motion step).

Table 19 lists the actual distance as calculated from the MR images at motion steps of 3 and 5 mm in the Y-axis right and left directions. Figures 52 and 53 show bar charts of the measured distance for bidirectional motion steps of 5 and 3 mm in the Y-axis, respectively, with respect to the repetition number for 10 repetitions. Figure 54 shows the mean values of the actual measured distance versus the intended distance for the Y axis right and left motion.

Table 39: List of distance measurements taken at motion step of 5, 3, and 10 mm for the Y-axis evaluation.

Intended distance (mm)	5		3		10
Measurement Number	**Distance moved left (mm)**	**Distance moved right (mm)**	**Distance moved left (mm)**	**Distance moved right (mm)**	**Distance moved left (mm)**
1	4.9221	4.3752	3.2814	2.7345	9.2973
2	4.9221	4.9221	2.7345	3.2814	-
3	4.9221	4.9221	3.2814	3.8283	-
4	4.9221	4.9221	3.2814	2.7345	-
5	4.9221	5.469	3.2814	3.2814	-
6	5.469	4.9221	3.2814	3.2814	-
7	4.3752	4.9221	2.7345	2.7345	-
8	5.469	4.9221	3.2814	3.2814	-
9	4.3752	4.9221	3.2814	3.2814	-
10	-	4.9221		2.7345	-
Average	**4.9221**	**4.9221**	**3.1599**	**3.1173**	**-**
Standard deviation	**0.3867**	**0.2578**	**0.2412**	**0.3691**	**-**

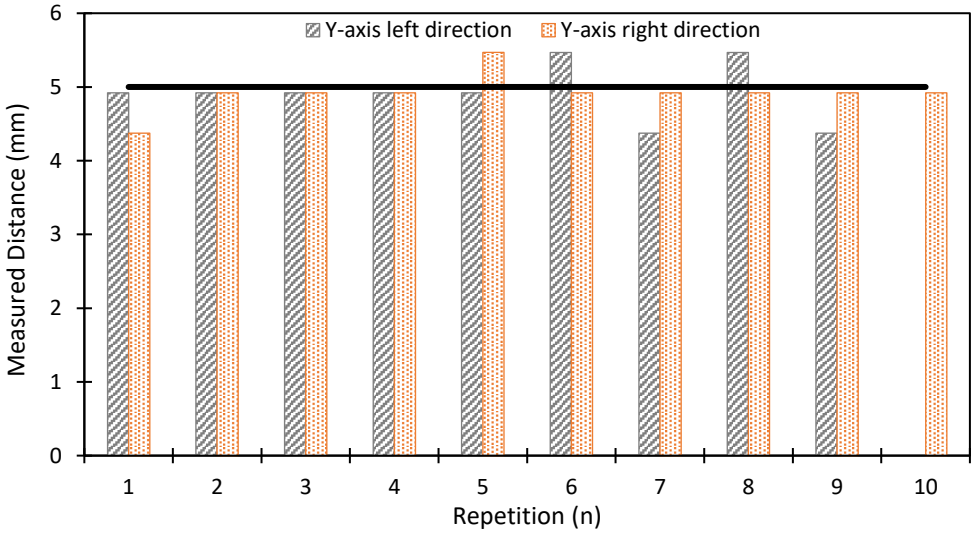

Figure 52: Distance measurements for 10 repetitions for movement step of 5 mm in the Y-axis left and right directions. The black straight line indicates the intended distance.

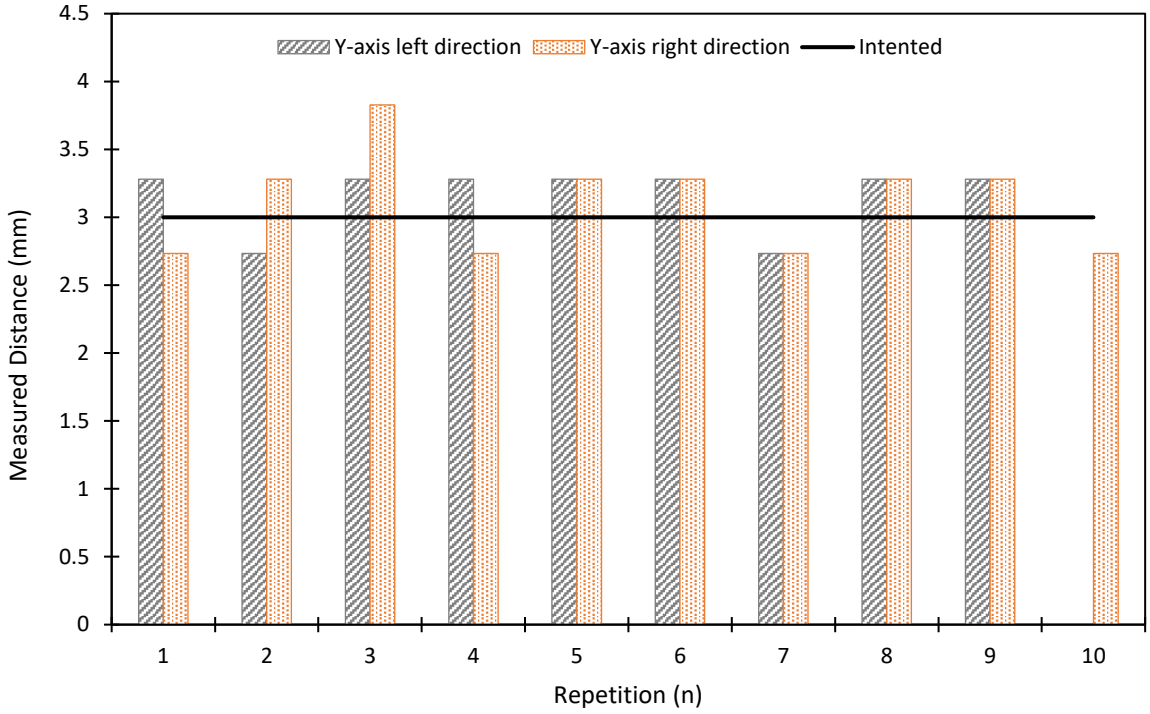

Figure 53: Distance measurements for 10 repetitions for movement step of 3 mm in the Y-axis left and right directions. The black straight line indicates the intended distance.

Figure 54: Mean value of the measured distance versus intended distance for the Y-axis left and right motions. Error bars correspond to the standard deviation.

The motion error was estimated for each motion step in both Y-axis directions. Notably, the motion step of 10 mm was tested just to show that the robot can move at a further distance. Table 20 summarizes the error measured at motion steps of 5 and 3 mm for the Y-axis left and right directions.

Table 20: List of error estimated at different motion steps for the Y-axis left and right directions.

Step (mm)	Error-left motion (µm)	Error-left motion (%)	Error-right motion (µm)	Error-right motion (%)
5	77.900	1.558	77.900	1.558
3	159.867	5.329	117.330	3.911
10	702.700	7.027	-	-

Evaluation of the motion accuracy using a visual method

The motion accuracy was also assessed through visual observations of multiple ablations produced on a transparent plastic film (0.9 mm thickness, FDM400mc print plate, Stratasys Ltd.) using the robotic system version 2. A spherically focused transducer (frequency: 1.1 MHz, diameter: 50 mm, focal length: 70 mm, Medsonic Ltd., Limassol, Cyprus) was used. The water enclosure containing the transducer was filled with degassed water up to the plastic film. Lesion formation was a result of ultrasonic reflection at the plastic/air interface. The transducer was moved to sonicate the film in square grid patterns for evaluating the accuracy of motion, as well as the linear motion alignment in the X and Y axes. An acoustic power of 10.5 W was applied at each grid point using an RF amplifier (AG1012, T & C Power Conversion, Inc., Humboldt St., Rochester, NY). The sonication time varied from 1-4 s so as to control the lesion size. Subsequently, sonications were performed with varying motion step and sonication time, and the time delay between successive sonications was set at 30 s. Also, the maximum motion range of the positioning mechanism in the horizontal plane was estimated by applying sonications at the extreme points of movement in the X and Y axes. The experimental set-up and the concept of the experiment are shown in Figures 55 and 56, respectively.

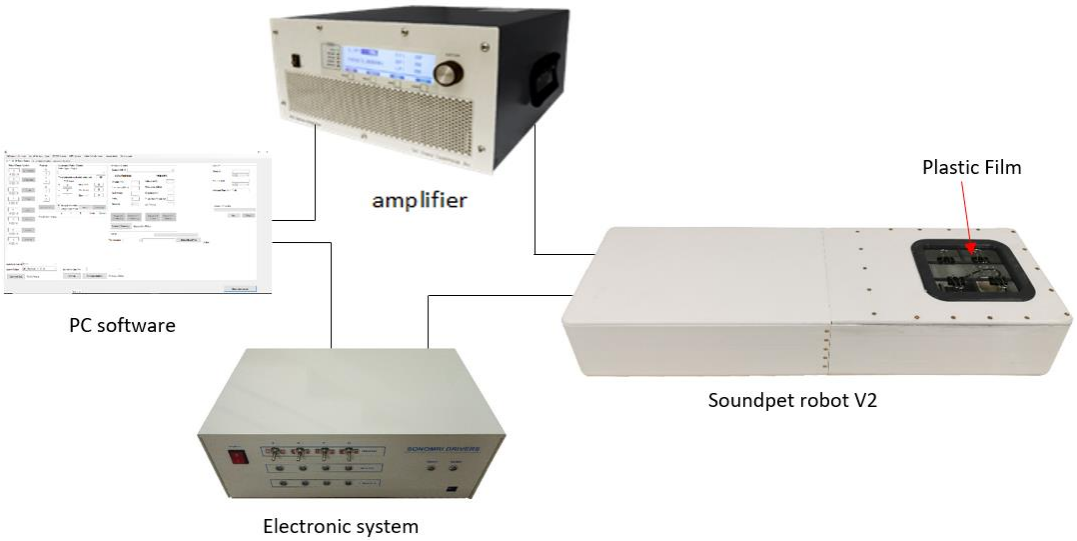

Figure 55: Experimental set-up that was used to create multiple lesions on plastic films.

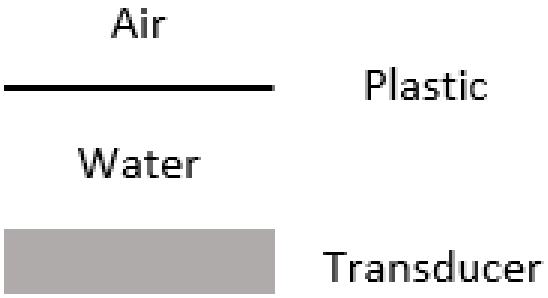

Figure 56: Concept of the experiment.

The appropriate selection of sonication time and grid step allowed formation of discrete and overlapping lesions and visual evaluation of the accuracy of motion and alignment. Experiments were conducted on 10 plastic films with varying grid pattern, step size, and sonication time.

1st plastic film: A 4x1 grid pattern with a step distance of 10 mm and a time delay of 30 s between each sonication was performed on the plastic film. Sonications were performed using an acoustic power of 10.5 W (electric power 30 W) for 4, 3, 2 and 1 s, sequentially. The distance between the transducer and the upper surface of the plastic film was set at 4.5 cm. Figure 57A shows the plastic film after the multiple sonications while Figure 57B shows the order with which the 4x1 grid pattern was executed.

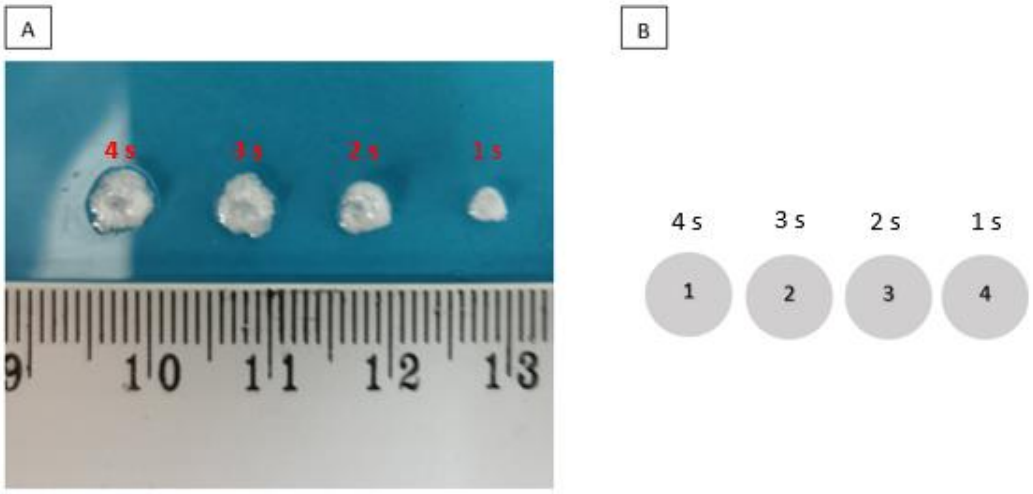

Figure 57: a) Lesions formed on the film after exposure at acoustic power of 10.5 W (electric power 30 W). The distance between the upper surface of the plastic film and the transducer ID 24 was 4.5 cm, and b) The grid pattern that was followed. Lesions 1, 2, 3 and 4 correspond to sonication times of 4, 3, 2, and 1 s, respectively. The step distance was 10 mm.

2nd plastic film: A 6x5 grid pattern with a step distance of 5 mm and a time delay of 30 s between each sonication was performed on the plastic film. An acoustic power of 10.5 W (electric power 30 W) was applied for a sonication time of 1 s. The distance between the transducer and the upper surface of the plastic film was set at 4.5 cm. Figure 58A shows the plastic film after the multiple sonications while Figure 58B shows the order with which the 6x5 grid pattern was executed.

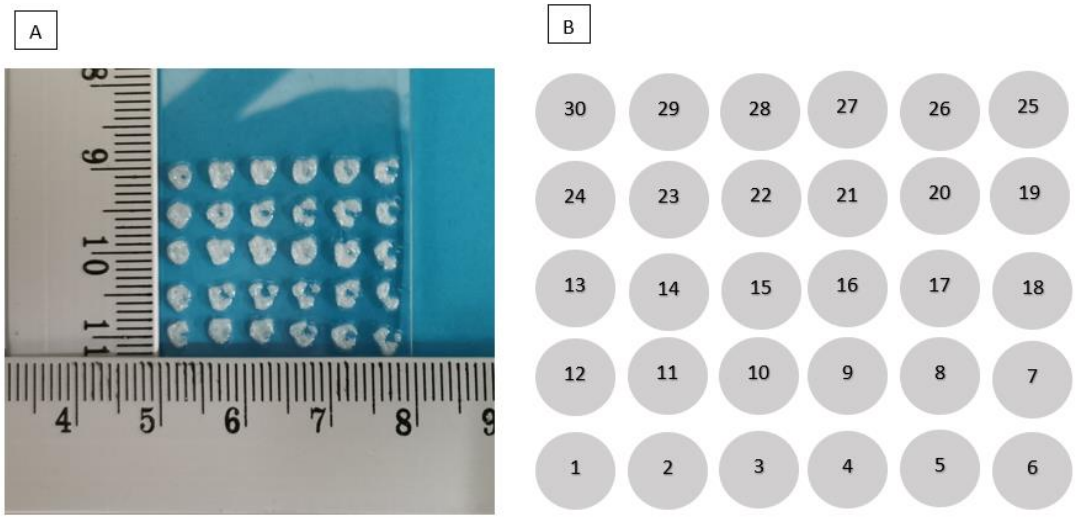

Figure 58: a) Lesions formed on the plastic film after exposure at acoustic power of 10.5 W (electric power 30 W) for a sonication time of 1 s. The distance between the upper surface of the plastic film and the transducer ID 24 was 4.5 cm, and b) The grid pattern that was followed. The step distance was 5 mm.

3rd plastic film: A 5x3 grid pattern with a step distance of 10 mm and a time delay of 30 s between each sonication was performed on the plastic film. An acoustic power of 10.5 W (electric power 30 W) was applied for a sonication time of 1 s. The distance between the transducer and the upper surface of the plastic film was set at 4.5 cm. Figure 59A shows the plastic film after the multiple sonications while Figure 59B shows the order with which the 5x3 grid pattern was executed.

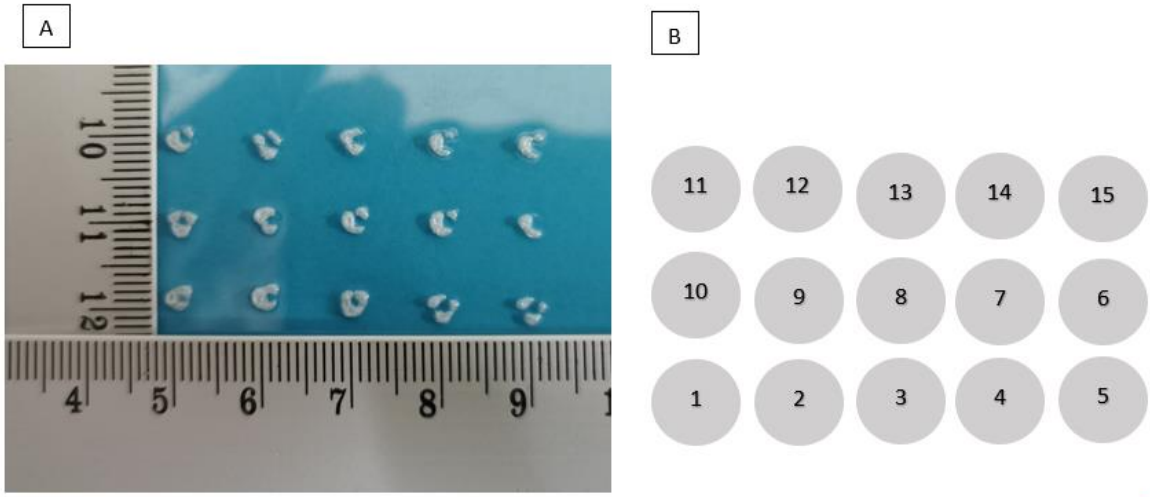

Figure 59: a) Lesions formed on the plastic film after exposure at acoustic power of 10.5 W (electric power 30 W) for a sonication time of 1 s. The distance between the upper surface of the plastic film and the transducer ID 24 was 4.5 cm, and b) The grid pattern that was followed. The step distance was 10 mm.

4th plastic film: Four sonications were performed at the extreme points of movement in the X and Y axes, to determine the available motion range in the horizontal plane. The sonications were performed using an acoustic power of 10.5 W (electric power 30 W) for a sonication time of 1 s. The distance between the transducer and the upper surface of the plastic film was set at 4.5 cm. Figure 60A shows the plastic film after the sonications while Figure 60B shows the order with which the sonications were executed. The maximum motion range of the robotic system version 2 was found to be 6 cm in the X-axis and 7 cm in the Y-axis. The motion range is indicated in Figure 61.

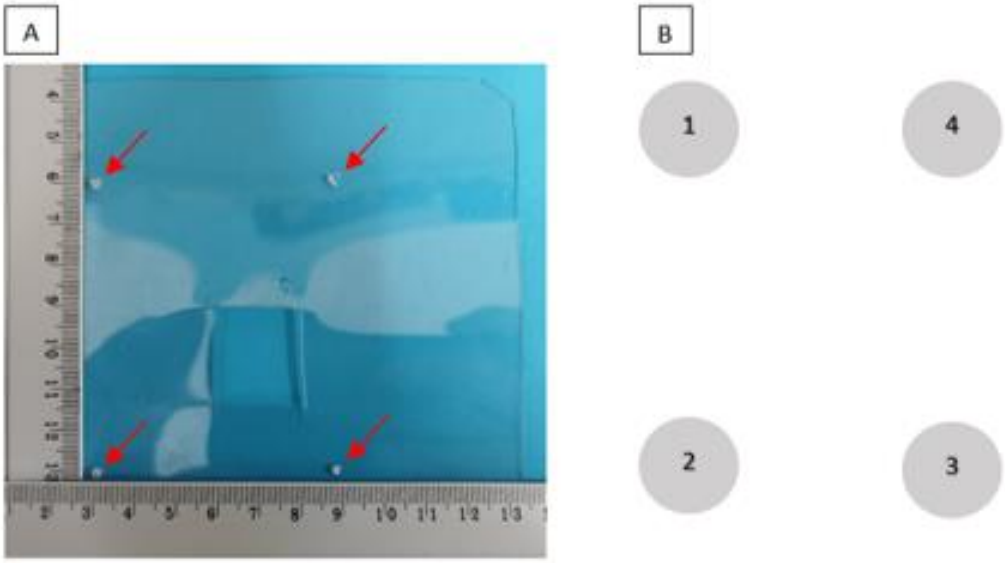

Figure 60: a) Lesions formed on the plastic film after exposure at acoustic power of 10.5 W (electric power 30 W) for a sonication time of 1 s. The distance between the upper surface of the plastic film and the transducer ID 24 was 4.5 cm, and b) The order that was followed for the sonications.

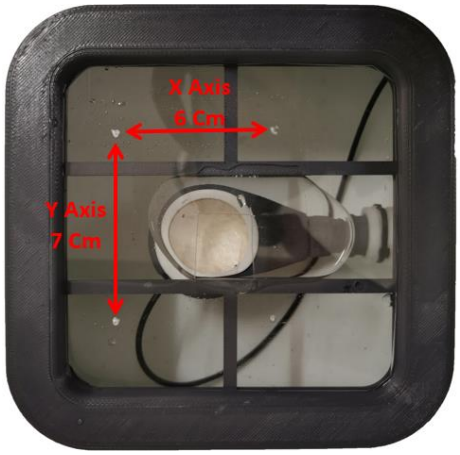

Figure 61: Maximum motion range of the robotic system version 2.

5th plastic film: A 11x15 grid pattern with a step distance of 5 mm and a time delay of 30 s between each sonication was performed on the plastic film. An acoustic power of 10.5 W (electric power 30 W) was applied for a sonication time of 1 s. The distance between the transducer and the upper surface of the plastic film was set at 4.5 cm. Figure 62A shows the plastic film after the multiple sonications while Figure 62B shows the order with which the 11x15 grid pattern was executed.

A

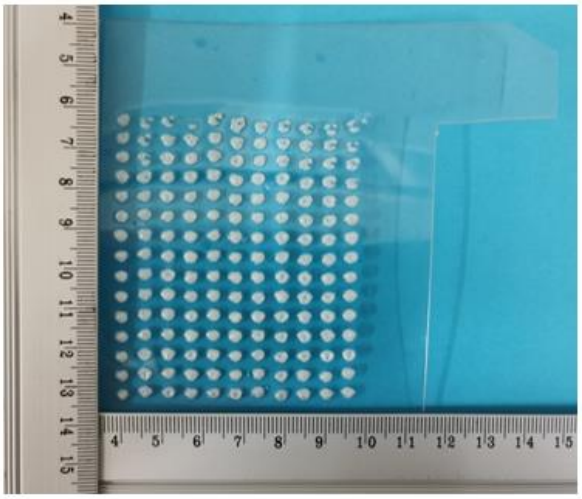

B

1	16	31	46	61	76	91	106	121	136	151
2	17	32	47	62	77	92	107	122	137	152
3	18	33	48	63	78	93	108	123	138	153
4	19	34	49	64	79	94	109	124	139	154
5	20	35	50	65	80	95	110	125	140	155
6	21	36	51	66	81	96	111	126	141	156
7	22	37	52	67	82	97	112	127	142	157
8	23	38	53	68	83	98	113	128	143	158
9	24	39	54	69	84	99	114	129	144	159
10	25	40	55	70	85	100	115	130	145	160
11	26	41	56	71	86	101	116	131	146	161
12	27	42	57	72	87	102	117	132	147	162
13	28	43	58	73	88	103	118	133	148	163
14	29	44	59	74	89	104	119	134	149	164
15	30	45	60	75	90	105	120	135	150	165

Figure 62: a) Lesions formed on the plastic film after exposure at acoustic power of 10.5 W (electric power 30 W) for a sonication time of 1 s. The distance between the upper surface of the plastic film and the transducer ID 24 was 4.5 cm, and b) The grid pattern that was followed. The step distance was 5 mm.

6th plastic film: A 10x10 grid pattern with a step distance of 2 mm and a time delay of 30 s between each sonication was performed on the plastic film. An acoustic power of 10.5 W (electric power 30 W) was applied for a sonication time of 1 s. The distance between the transducer and the upper surface of the plastic film was set at 4.5 cm. Figure 63A shows the plastic film after the multiple sonications while Figure 63B shows the order with which the 10x10 grid pattern was executed.

A

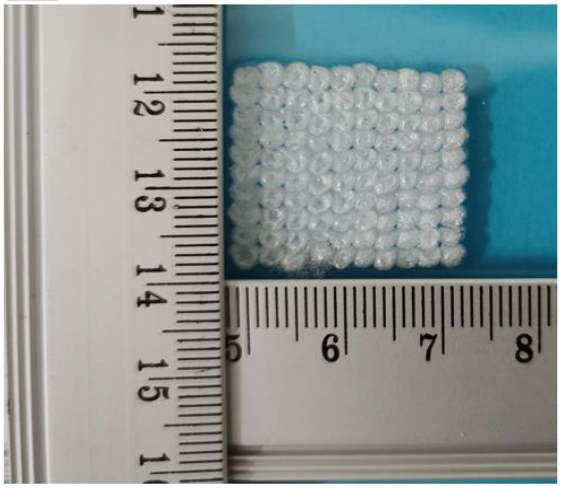

B

1	11	21	31	41	51	61	71	81	91
2	12	22	32	42	52	62	72	82	92
3	13	23	33	43	53	63	73	83	93
4	14	24	34	44	54	64	74	84	94
5	15	25	35	45	55	65	75	85	95
6	16	26	36	46	56	66	76	86	96
7	17	27	37	47	57	67	77	87	97
8	18	28	38	48	58	68	78	88	98
9	19	29	39	49	59	69	79	89	99
10	20	30	40	50	60	70	80	90	100

Figure 63: a) Lesions formed on the plastic film after exposure at acoustic power of 10.5 W (electric power 30 W) for a sonication time of 1 s. The distance between the upper surface of the plastic film and the transducer ID 24 was 4.5 cm, and b) The grid pattern that was followed. The step distance was 2 mm.

7th plastic film: A 10x10 grid pattern with a step distance of 2 mm and a time delay of 30 s between each sonication was performed on the plastic film. An acoustic power of 10.5 W (electric power 30 W) was applied for a sonication time of 1 s. The distance between the transducer and the upper surface of the plastic film was set at 4.5 cm. Figure 64A shows the plastic film after the multiple sonications while Figure 64B shows the order with which the 10x10 grid pattern was executed.

A

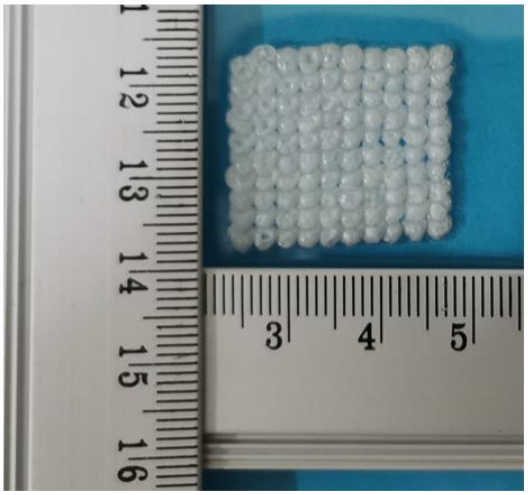

B

1	11	21	31	41	51	61	71	81	91
2	12	22	32	42	52	62	72	82	92
3	13	23	33	43	53	63	73	83	93
4	14	24	34	44	54	64	74	84	94
5	15	25	35	45	55	65	75	85	95
6	16	26	36	46	56	66	76	86	96
7	17	27	37	47	57	67	77	87	97
8	18	28	38	48	58	68	78	88	98
9	19	29	39	49	59	69	79	89	99
10	20	30	40	50	60	70	80	90	100

Figure 64: a) Lesions formed on the plastic film after exposure at acoustic power of 10.5 W (electric power 30 W) for a sonication time of 1 s. The distance between the upper surface of the plastic film and the transducer ID 24 was 4.5 cm, and b) The grid pattern that was followed. The step distance was 2 mm.

8th plastic film: A 10x10 grid pattern with a step distance of 2 mm and a time delay of 60 s between each sonication was performed on the plastic film. An acoustic power of 10.5 W (electric power 30 W) was applied for a sonication time of 2 s. The distance between the transducer and the upper surface of the plastic film was set at 4.5 cm. Figure 65A shows the plastic film after the multiple sonications while Figure 65B shows the order with which the 10x10 grid pattern was executed.

A

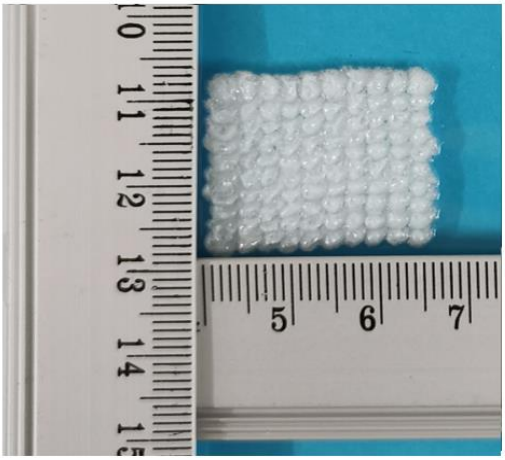

B

1	11	21	31	41	51	61	71	81	91
2	12	22	32	42	52	62	72	82	92
3	13	23	33	43	53	63	73	83	93
4	14	24	34	44	54	64	74	84	94
5	15	25	35	45	55	65	75	85	95
6	16	26	36	46	56	66	76	86	96
7	17	27	37	47	57	67	77	87	97
8	18	28	38	48	58	68	78	88	98
9	19	29	39	49	59	69	79	89	99
10	20	30	40	50	60	70	80	90	100

Figure 65: a) Lesions formed on the plastic film after exposure at acoustic power of 10.5 W (electric power 30 W) for a sonication time of 2 s. The distance between the upper surface of the plastic film and the transducer ID 24 was 4.5 cm, and b) The grid pattern that was followed. The step distance was 2 mm.

9th plastic film: A 15x15 grid pattern with a step distance of 2 mm and a time delay of 60 s between each sonication was performed on the plastic film. An acoustic power of 10.5 W (electric power 30 W) was applied for a sonication time of 3 s. The distance between the transducer and the upper surface of the plastic film was set at 4.5 cm. Figure 66A shows the plastic film after the multiple sonications while Figure 66B shows the order with which the 15x15 grid pattern was executed.

A

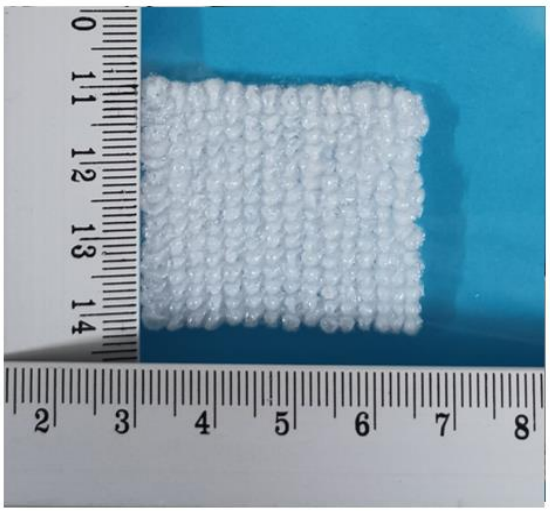

B

1	16	31	46	61	76	91	106	121	136	151	166	181	196	211
2	17	32	47	62	77	92	107	122	137	152	167	182	197	212
3	18	33	48	63	78	93	108	123	138	153	168	183	198	213
4	19	34	49	64	79	94	109	124	139	154	169	184	199	214
5	20	35	50	65	80	95	110	125	140	155	170	185	200	215
6	21	36	51	66	81	96	111	126	141	156	171	186	201	216
7	22	37	52	67	82	97	112	127	142	157	172	187	202	217
8	23	38	53	68	83	98	113	128	143	158	173	188	203	218
9	24	39	54	69	84	99	114	129	144	159	174	189	204	219
10	25	40	55	70	85	100	115	130	145	160	175	190	205	220
11	26	41	56	71	86	101	116	131	146	161	176	191	206	221
12	27	42	57	72	87	102	117	132	147	162	177	192	207	222
13	28	43	58	73	88	103	118	133	148	163	178	193	208	223
14	29	44	59	74	89	104	119	134	149	164	179	194	209	224
15	30	45	60	75	90	105	120	135	150	165	180	195	210	225

Figure 66: a) Lesions formed on the plastic film after exposure at acoustic power of 10.5 W (electric power 30 W) for a sonication time of 3 s. The distance between the upper surface of the plastic film and the transducer ID 24 was 4.5 cm, and b) The grid pattern that was followed. The step distance was 2 mm.

10th plastic film: A 15x15 grid pattern with a step distance of 2 mm and a time delay of 30 s between each sonication was performed on the plastic film. An acoustic power of 10.5 W (electric power 30 W) was applied for a sonication time of 3 s. The distance between the transducer and the upper surface of the plastic film was set at 4.5 cm. Figure 67A shows the plastic film after the multiple sonications while Figure 67B shows the order with which the 15x15 grid pattern was executed. Also, for this experiment, we used a plastic holder to secure the plastic film as shown in Figure 68.

A

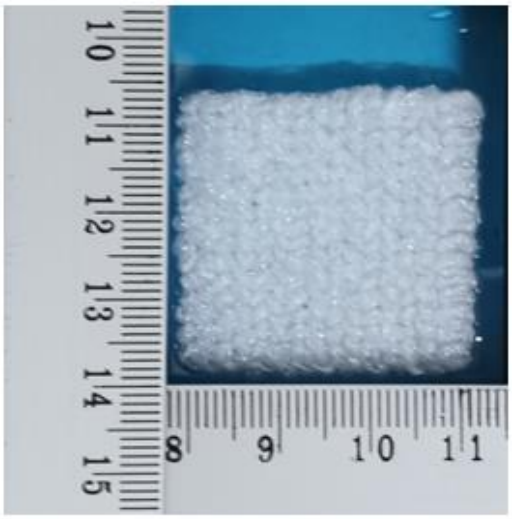

B

225	196	195	166	165	136	135	106	105	76	75	46	45	16	15
224	197	194	167	164	137	134	107	104	77	74	47	44	17	14
223	198	193	168	163	138	133	108	103	78	73	48	43	18	13
222	199	192	169	162	139	132	109	102	79	72	49	42	19	12
221	200	191	170	161	140	131	110	101	80	71	50	41	20	11
220	201	190	171	160	141	130	111	100	81	70	51	40	21	10
219	202	189	172	159	142	129	112	99	82	69	52	39	22	9
218	203	188	173	158	143	128	113	98	83	68	53	38	23	8
217	204	187	174	157	144	127	114	97	84	67	54	37	24	7
216	205	186	175	156	145	126	115	96	85	66	55	36	25	6
215	206	185	176	155	146	125	116	95	86	65	56	35	26	5
214	207	184	177	154	147	124	117	94	87	64	57	34	27	4
213	208	183	178	153	148	123	118	93	88	63	58	33	28	3
212	209	182	179	152	149	122	119	92	89	62	59	32	29	2
211	210	181	180	151	150	121	120	91	90	61	60	31	30	1

Figure 67: a) Lesions formed on the plastic film after exposure at acoustic power of 10.5 W (electric power 30 W) for a sonication time of 3 s. The distance between the upper surface of the plastic film and the transducer ID 24 was 4.5 cm, and b) The grid pattern that was followed. The step distance was 2 mm.

Figure 68: Photo of the plastic holder that holds the plastic film.

Discussion

The accuracy of motion of the 4 DOF robotic systems was evaluated for both linear (in all axes) and angular motions using three different methods (digital calipers, MRI, visual technique). The accuracy of the linear motion was tested at motion steps of 1 mm, 5 mm, and 10 mm using digital calipers and specially designed 3D-printed parts.

The motion error was estimated for each motion step and each direction of the X, Y, and Z axes. For the robotic system version 1, at motion step of 1 mm in the X-axis, the error of the reverse motion was greater than that of the forward motion. At motion step of 5 mm, the error of the reverse motion was also greater than that of the forward motion, and notably, it was the highest error of all tested motion steps in the X-axis. At motion step of 10 mm, the error of the X-axis forward and reverse directions was almost the same. Overall, the error of the Y-axis motion was higher than that of the X and Z axes. At motion step of 1 mm, the error of the left motion was smaller than the error of the right motion. On the contrary, the motion step of 5 mm resulted in about the same error in both directions. The motion error in the right direction at a motion step of 10 mm was the highest of all the linear axes and directions. For the Z-axis, the error at motion steps of 1 and 5 mm was significantly low while the error at 10 mm motion step was slightly higher. In summary, the 1 mm motion in the X-axis resulted in a maximum error of 53 μm (reverse direction). For the 5 mm motion step, the maximum error was 114 μm for the same direction. For the Y-axis, the maximum estimated motion error was 127 μm for the 1 mm step (right direction) and 660 μm for the 5 mm step (left direction). For the Z-axis, the maximum error was found for the 10 mm step in the down direction, and it was 84 μm.

The accuracy of the angular motion was also assessed using an angle caliper and specially designed 3D-printed parts. The error of angular motion in the CW direction was approximately the same as the error in the CCW direction. The error of angular motion for both CW and CCW directions was higher at angular step of 10^{o} than at angular steps of 1^{o} and 5^{o}. In addition, the error of angular motion slightly increased with the increase of the angular step. Lastly, the speed of angular motion was almost the same in the CW (143.25 ^{o}/s) and CCW (138.64 ^{o}/s) directions.

Moreover, the motion speed of the robotic device version 1 in all linear axes (X, Y and Z) and directions was also calculated. The activation time of the motors during motion execution was measured through the Arduino microcontroller and displayed on the software interface. Motion

speed depends mainly on the drivers and each driver can control the motors at different speeds. However, the motion of the motors, and therefore, the distance of motion in the various axes is not affected by the speed setting parameter of the drivers. Generally, there was no significant difference between the speed of bidirectional motions (forward/reverse, right/left, up/down). The speed in the forward direction of the X-axis, right direction of the Y-axis, and up direction of Z-axis was 10.12 mm/s, 14.37 mm/s, and 9.82 mm/s, respectively. The speed in the reverse direction of the X-axis, left direction of the Y-axis, and down direction of the Z-axis was 9.88 mm/s, 14.8 mm/s, and 9.7 mm/s, respectively. The fastest linear motion was found for the Y-axis. The high speed can adversely affect the motion accuracy of the robotic device, and this could be a reason for the higher motion error that was measured in the Y-axis. Figure 69 summarizes the mean value of the actual measured distance versus the intended distance for all linear axes and directions of motion of the robotic system version 1. Table 21 summarizes the motion accuracy results for the 4 DOF robotic device version 1.

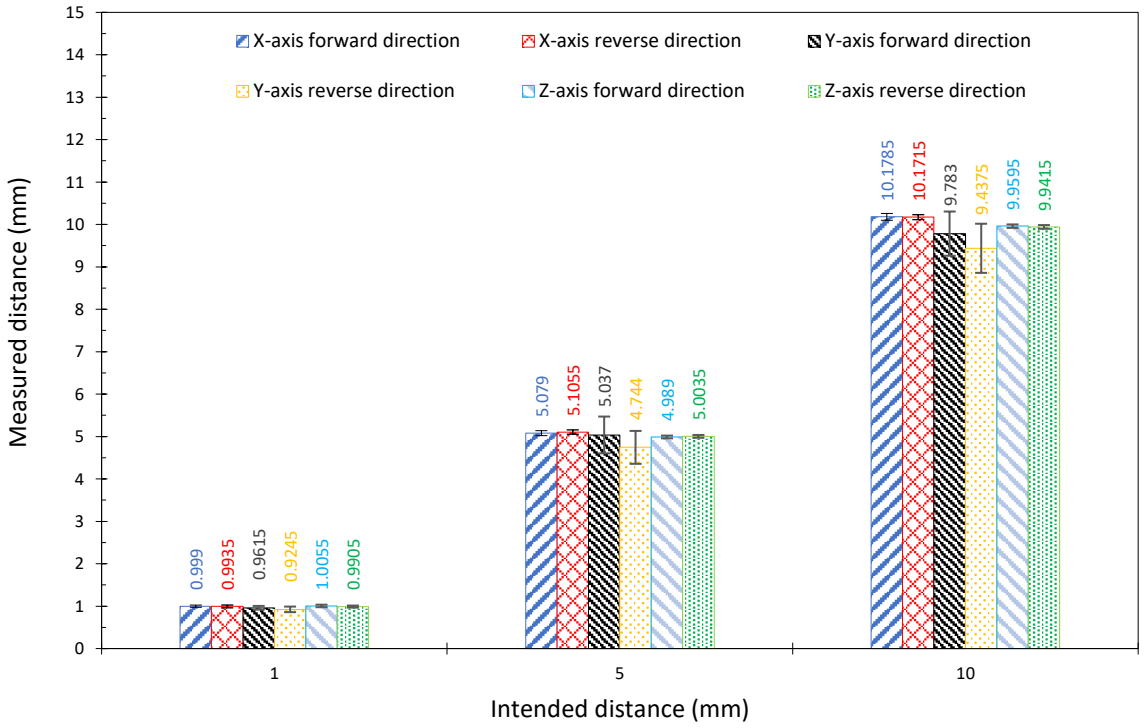

Figure 69: Mean value of the measured distance versus intended distance for all axes and directions of motion (robotic system version 1).

Table 21: Results of the motion accuracy evaluation of the 4 DOF robotic device version 1.

Linear axis	**Step (mm)**	**Range (mm)**	**Error forward (µm)**	**Error reverse (µm)**	**Speed forward (mm/s)**	**Speed reverse (mm/s)**
x	1	0.9-1.13	39	53	10.31	10.05
	5	4.87-5.35	94	114	10.43	9.80
	10	9.88-10.47	206	172	10.01	9.98
y	**Step (mm)**	**Range (mm)**	**Error right (µm)**	**Error left (µm)**	**Speed right (mm/s)**	**Speed left (mm/s)**
	1	0.74-1.19	127	76	14.28	15.93
	5	3.45-7.35	640	660	13.84	14.16
	10	8.02-12.38	1177	926	14.66	14.46
z	**Step (mm)**	**Range (mm)**	**Error up (µm)**	**Error down (µm)**	**Speed up (mm/s)**	**Speed down (mm/s)**
	1	0.89-1.11	52	39	9.90	10.09
	5	4.9-5.11	55	55	9.90	9.73
	10	9.78-10.11	69	84	9.78	9.59
Angular axis	**Step (degrees)**	**Range (degrees)**	**Error CW (degrees)**	**Error CCW (degrees)**	**Speed CW (º/s)**	**Speed CCW (º/s)**
θ	1	0.8-1.3	0.1	0.155	132.43	118.78
	5	4.7-5.7	0.25	0.245	144.5	145.13
	10	9.9-10.7	0.32	0.29	148.42	144.46

The maximum motion error of the robotic system version 2 was found in the Y-axis right direction, and it was 123 µm. Generally, the motion of the robotic system version 2 was more accurate than that of the robotic system version 1. Figure 70 summarizes the mean value of the actual measured distance versus the intended distance for both directions of the X and Y axes of the robotic system version 2. Table 22 summarizes the motion accuracy results for the 4 DOF robotic device version 2.

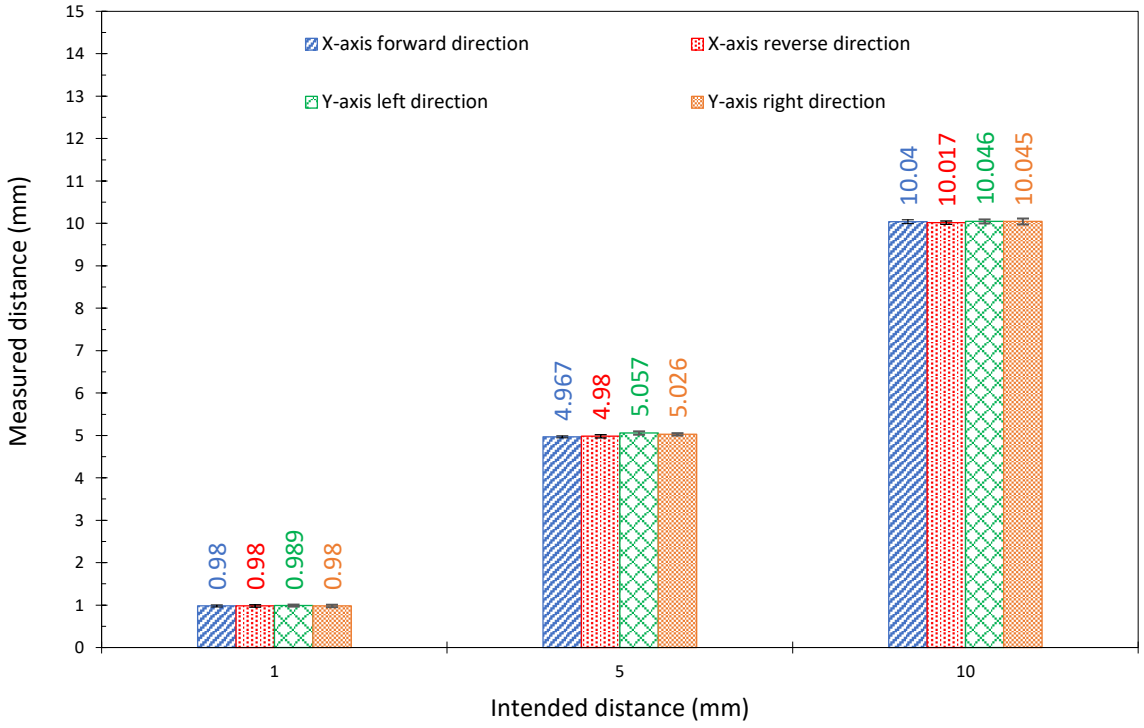

Figure 70: Mean value of the measured distance versus intended distance for all axes and directions of motion (robotic system version 2).

Table 22: Results of the motion accuracy evaluation of the 4 DOF robotic device version 2.

Linear axis	**Step (mm)**	**Range (mm)**	**Error forward (µm)**	**Error reverse (µm)**
x	1	0.88-1.08	42	51
	5	4.85-5.15	47	65
	10	9.78-10.19	81	58
y	**Step (mm)**	**Range (mm)**	**Error right (µm)**	**Error left (µm)**
	1	0.88-1.09	45	42
	5	4.89-5.19	53	84
	10	9.85-10.29	123	86

Figure 71 summarizes the mean value of the actual measured distance versus intended distance for the X and Y axes bidirectional motions of the robotic system version 2, as calculated from the MRI-based motion accuracy method. Table 23 summarizes the range of measured distance and the corresponding motion errors at different commanded motion steps in both directions of the X and Y axes.

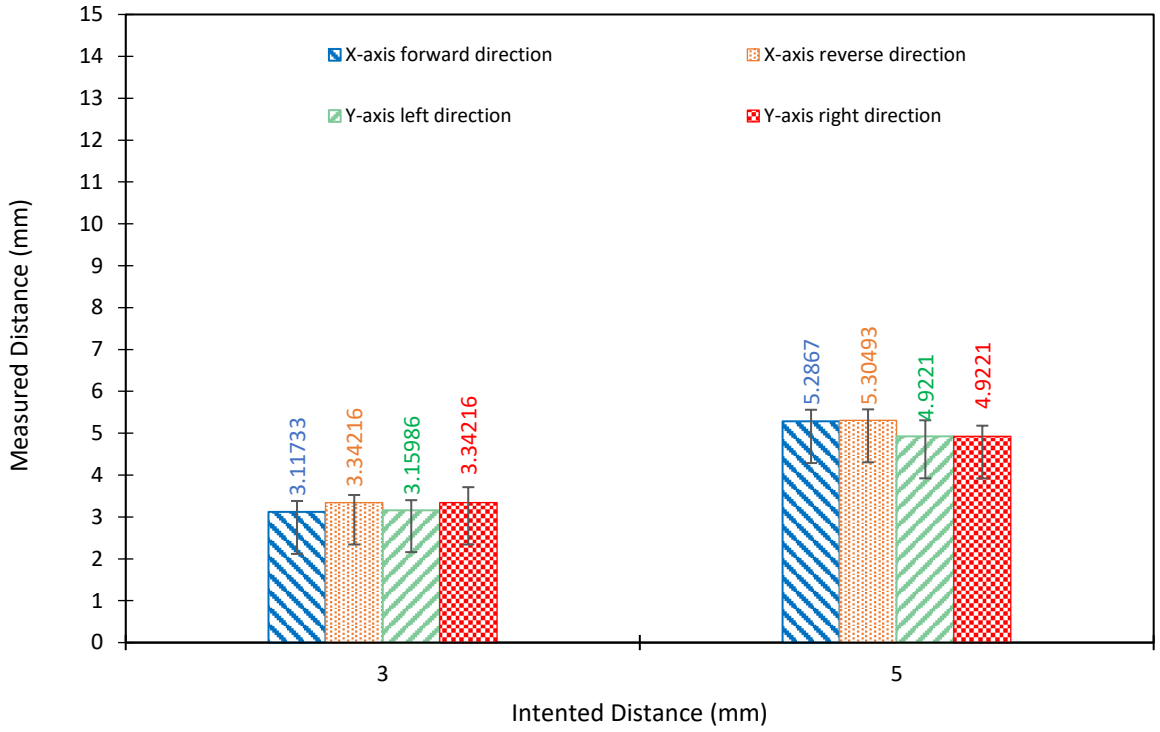

Figure 71: Mean value of the measured distance versus intended distance for the X and Y axes bidirectional motions (robotic system version 2), as calculated using the MRI method.

Table 23: Results of the motion accuracy MRI evaluation of the 4 DOF robotic device version 2.

Linear axis	Step (mm)	Range (mm)	Error forward (μm)	Error reverse (μm)
x	5	4.9221-5.469	286.7	304.93
	3	2.7345-3.8283	117.33	342.17
y			Error right (μm)	Error left (μm)
	5	4.3752-5.469	77.9	77.9
	3	2.7345-3.8283	117.33	159.87
	10	-	-	702.7

Three simple and practical methods for assessing the accuracy of motion of the robotic device (version 2/final version) were described. All the methods were based on the idea of evaluating the performance of the device in accurately executing commanded movements.

Firstly, the motion accuracy of the robotic device was evaluated using digital calipers integrated on the motion stages under evaluation using specially designed 3D printed structures. The mean error of linear motion varied from 0.042 ± 0.032 mm for the 1 mm step

in the X axis forward direction to 0.123 ± 0.082 mm for the 10 mm step in the Y axis right direction. Accordingly, the mean error of angular motion varied from a minimum value of 0.100 ± 0.077^{o} for the 1^{o} step to a maximum value of 0.320 ± 0.225^{o} for the 10^{o} step (CW rotation). Contrary to the findings of a previous study [17], the mean error was found to be increasing with increasing motion step for all four axes.

In comparison with previous designs [10-11][17][20], the principle of movement of the proposed one was significantly improved by the dual encoder positioning control that guarantees a smooth, reliable, and highly accurate motion in all stages. Additionally, the problem of reduced accuracy for small steps previously observed [17] seems to be solved by using faster software commends that makes the encoders' reading more accurate.

The system was then evaluated in the MRI environment that is intended to be used. The accuracy of motion remains satisfactory during full operation of the system in the MRI environment. Additionally, there was no evidence of any magnetically induced shift of the mechanical components that could compromise the accuracy of ultrasound delivery to the target, and therefore the patient's safety in potential future clinical applications.

The spatial positioning errors estimated by the benchtop setting using digital calipers are significantly smaller than those obtained in the MRI setting. This is attributed to the size of voxels of the MR images that determine the finest possible accuracy. Given the MRI resolution of 0.55 mm per pixel, the estimated motion errors are within a reasonable range. Although this approach suffers from imaging resolution limitations, a smaller pixel could provide more precise distance estimates, but at the cost of increased image acquisition time and reduced signal to noise ratio (SNR).

The high degree of accuracy evidenced by benchtop testing with calipers was also confirmed by multiple ablations on a transparent plastic film. The melted spots formed after grid ablation were arranged in a discrete pattern, in a highly accurate manner, clearly demonstrating that the linear stages were moved with the commanded step. As observed, the centers of almost all the spots were equally spaced, demonstrating excellent repeatability. Multiple ablations in a grid with a smaller spatial step between adjacent sonications and three times longer sonication time resulted in a well-defined square area of overlapping lesions. The results suggest that the system can precisely ablate a large tissue volume by overlapping lesions.

The aforementioned ablation method is intended specifically for testing the accuracy of FUS systems and is essential for assessing their ability to precisely deliver heating spots along the

desired pattern. However, it is notable that in such systems the accuracy in free robot workspace is representative of that in more realistic scenarios (phantom and *in vivo* experiments), whereas for instance, in needle-based interventions is not. This is consistent with what has been previously reported by Price et al. [9], who found that the intrinsic accuracy of a FUS system as estimated in the air was similar to that obtained by phantom experiments in the MRI setting.

The proposed methods were greatly improved in terms of accuracy compared to those we have previously used [10-11], [21-22]. The quality of benchtop evaluation was enhanced by using 3D printed structures specially designed for each individual axis, which provided perfect alignment of the caliper with each axis of measurement and reduced systematic errors [10]. Regarding the MRI evaluation, the accuracy of step movement has been previously estimated by locating the transducer on MR images [22]. Advantageously, a more accurate method is proposed herein, involving the use of a 2 mm plastic marker, which is clearly visible on MRI images using the appropriate sequence.

Overall, the accuracy of the tested robotic device, as proven by all three methods, is sufficient to guarantee an efficient performance of the system in terms of precise ablation in both laboratory and MRI environments. We believe the three methods proposed should serve as the standard methods for evaluating FUS robotic systems.

References

[1] B. S. Peters, P. R. Armijo, C. Krause, S. A. Choudhury, and D. Oleynikov, "Review of emerging surgical robotic technology," *Surg. Endosc.*, vol. 32, no. 4, pp. 1636–1655, 2018, doi: 10.1007/s00464-018-6079-2.t

[2] K. G. Chan, T. Fielding, and M. Anvari, "An image-guided automated robot for MRI breast biopsy," *Int. J. Med. Robot. Comput. Assist. Surg.*, vol. 12, no. 3, pp. 461–477, 2016, doi: 10.1002/rcs.

[3] A. Patriciu, D. Petrisor, M. Muntener, D. Mazilu, M. Schär, and D. Stoianovici, "Automatic Brachytherapy Seed Placement Under MRI Guidance," *IEEE Trans Biomed Eng*, vol. 54, no. 8, pp. 1499–1506, 2007, doi: 10.1109/TBME.2007.900816.

[4] N. Patel, J. Yan, R. Monfaredi, K. Sharma, K. Cleary, and I. Iordachita, "Preclinical evaluation of an integrated robotic system for magnetic resonance imaging guided shoulder arthrography," *Med. Imaging*, vol. 6, no. 2, 2019, doi: 10.1117/1.JMI.6.2.025006.

[5] H. Dou, S. Jiang, Z. Yang, L. Sun, X. Ma, and B. Huo, "Design and validation of a CT-guided robotic system for lung cancer brachytherapy:," *Med. Phys.*, vol. 44, no. 9, pp. 4828–4837, 2017, doi: 10.1002/mp.12435.

[6] M. A. Tavallaei, P. M. Johnson, J. Liu, and M. Drangova, "Design and evaluation of an MRI-compatible linear motion stage," *Med. Phys.*, vol. 43, no. 1, pp. 62–71, 2016, doi: 10.1118/1.4937780.

[7] Y. Koseki, T. Washio, K. Chinzei, and H. Iseki, "Endoscope Manipulator for Trans-nasal Neurosurgery, Optimized for and Compatible to Vertical Field Open MRI," *Med. Image Comput. Comput. Interv. — MICCAI 2002. MICCAI 2002. Lect. Notes Comput. Sci. Springer, Berlin, Heidelberg.*, vol. 2488, pp. 114–121, 2002.

[8] V. Groenhuis, F. J. Siepel, J. Veltman, J. K. van Zandwijk, and S. Stramigioli, "Stormram 4: An MR Safe Robotic System for Breast Biopsy," *Ann. Biomed. Eng.*, vol. 46, no. 10, pp. 1686–1696, 2018, doi: 10.1007/s10439-018-2051-5.

[9] K. D. Price *et al.*, "Design and validation of an MR-conditional robot for transcranial focused ultrasound surgery in infants," *Med. Phys.*, vol. 43, no. 9, pp. 4983–4995, 2016, doi: 10.1118/1.4955174.

[10] C. Yiallouras, N. Mylonas, and C. Damianou, “MRI-compatible positioning device for guiding a focused ultrasound system for transrectal treatment of prostate cancer,” *Int. J. Comput. Assist. Radiol. Surg.*, vol. 9, no. 4, pp. 745–753, 2014, doi: 10.1007/s11548-013-0964-x.

[11] C. Yiallouras, K. Ioannides, T. Dadakova, M. Pavlina, M. Bock, and C. Damianou, “Three-axis MR-conditional robot for high-intensity focused ultrasound for treating prostate diseases transrectally,” *J. Ther. Ultrasound*, vol. 3, no. 1, pp. 1–10, 2015, doi: 10.1186/s40349-014-0023-2.

[12] N. A. Patel *et al.*, “An Integrated Robotic System for MRI-Guided Neuroablation: Preclinical Evaluation,” *IEEE Trans Biomed Eng*, vol. 67, no. 10, pp. 2990–2999, 2020.

[13] A. Krieger *et al.*, “Development and Evaluation of an Actuated MRI-Compatible Robotic System for MRI-Guided Prostate Intervention,” *IEEE ASME Trans Mechatron*, vol. 18, no. 1, pp. 273–284, 2013, doi: 10.1109/TMECH.2011.2163523.

[14] J. G. A. Moreau-gaudry, N. Hungr, and A. Moreau-gaudry, “Evaluation of the Needle Positioning Accuracy of a Light Puncture Robot Under MRI Guidance: Results of a Clinical Trial on Healthy Volunteers,” *Cardiovasc Interv. Radiol*, vol. 41, no. 9, pp. 1428–1435, 2018, doi: 10.1007/s00270-018-2001-5.

[15] C. Yiallouras and C. Damianou, “Review of MRI positioning devices for guiding focused ultrasound systems,” *Int. J. Med. Robot. Comput. Assist. Surg.*, vol. 11, pp. 247–255, 2015.

[16] T. Wu, “A quality control program for MR-guided focused ultrasound ablation therapy,” *J. Appl. Clin. Med. Phys.*, vol. 3, no. 2, p. 162, 2002, doi: 10.1120/1.1459262.

[17] N. Mylonas and C. Damianou, “MR compatible positioning device for guiding a focused ultrasound system for the treatment of brain deseases,” *Int. J. Med. Robot. Comput. Assist. Surg.*, vol. 10, pp. 1–10, 2014.

[18] G. Sagias, C. Yiallouras, K. Ioannides, and C. Damianou, “An MRI-conditional motion phantom for the evaluation of high-intensity focused ultrasound protocols,” *Int. J. Med. Robot. Comput. Assist. Surger*, vol. 12, pp. 431–441, 2016.

[19] C. Y. An, J. H. Syu, C. S. Tseng, and C. J. Chang, “An ultrasound imaging-guided robotic HIFU ablation experimental system and accuracy evaluations,” *Appl. Bionics Biomech.*, vol. 2017, 2017, doi: 10.1155/2017/5868695.

[20] C. Damianou, K. Ioannides, and N. Milonas, “Positioning device for MRI-guided high intensity focused ultrasound system,” *Int. J. Comput. Assist. Radiol. Surg.*, vol. 2, no. 6, pp. 335–345, 2008, doi: 10.1007/s11548-007-0145-x.

[21] E. Epaminonda, T. Drakos, C. Kalogirou, M. Theodoulou, C. Yiallouras, and C. Damianou, “MRI guided focused ultrasound robotic system for the treatment of gynaecological tumors,” *Int. J. Med. Robot. Comput. Assist. Surg.*, vol. 12, pp. 46–52, 2016.

[22] M. Yiannakou, G. Menikou, C. Yiallouras, C. Ioannides, and C. Damianou, “MRI guided focused ultrasound robotic system for animal experiments,” *Int. J. Med. Robot. Comput. Assist. Surg.*, vol. 13, no. 4, 2017.